Anisotropic Damage and Visco-Elasto-Plasticity Applied to Multiphasic Materials

Alain Sellier

Anisotropic Damage and Visco-Elasto-Plasticity Applied to Multiphasic Materials

FLUENDO3D Version 24-A

Technical Report[1]

Alain Sellier[2]

February 22, 2018

[1]LMDC, Université de Toulouse, INSA/UPS Génie Civil, 135 Avenue de Rangueil, 31077 Toulouse cedex 04 France.
[2]alain.sellier@univ-tlse3.fr

Contents

List of Tables

List of Figures

Part I

Introduction

General Principles

This document describes the constitutive equations currently implemented in the numerical model FLUENDO3D. This model, clarified in LMDC Toulouse, is dedicated to the numerical simulation of non linear behaviour of matrix reinforced by distributed reinforcements. The matrix behaviour law considers both localised and diffuse damages, permanent strains induced by creep or plasticity, and effects of pressures in its porosity. The pressures can be induced by water dying or internal swelling reactions. Different reinforcements can be considered simultaneously. Each of them is oriented and acts on the matrix either thanks to a perfect bond or by a sliding interface. The reinforcement's behaviour includes permanent strains induced by plasticity or relaxation. The matrix cracking is simulated resorting to the damage theory. The distributed crack method is used. The model supplies the localised cracks orientations and openings. It can also consider presence of defects in the matrix thanks to a theory based on probabilistic considerations. The different components of this model can work alone or together, depending on the user's intentions. For instance if the damage module is not required all the other modules stay active invoking the model with the FLUAGE3D command instead of FLUENDO3D command. On the contrary if the creep modules are not needed the ENDO3D command allows to skip the creep modules and keep the damage ones. However, the plastic modules and the chemical modules are always active. But, of course, if data relative to the chemical modules are omitted by the users the corresponding module are dis-activated automatically. Concerning distributed reinforcements types, their number can be chosen between 0 (none reinforcements) and 5. More reinforcements types could be considered but a re-compilation of the model should be done with adequate parameters.

Main features

The different features available in this model are summarized below. The constitutive equations corresponding to each item are supplied in next chapters. The data list and the internal variables list corresponding to each phenomenon are summarized at the end of the document.

- Non-linear mechanics
  - Plasticity
    - Rotating orthotropic Rankine criteria for tensile stresses
    - Rotating orthotropic Rankine criteria for localised cracks re-closure
    - Rotating orthotropic Rankine criteria for poro-mechanic internal pressure
    - Drucker Pragger criterion
  - Damage
    - Orthotropic damage in tension coupled with plasticity Rankine criteria
    - Fracture energy management based on an anisotropic Hillerborgh method
    - Isotropic damage coupled with Drucker Pragger plasticity
    - Isotropic thermal damage
  - Non-linear viscosity
    - Reversible creep based on Visco-elasticity
    - Permanent creep based on non linear viscosity
    - Anisotropic induced creep rates based on anisotrpic consolidation theory
- Chemo-mechanical couplings
  - Hydration effects
  - Water content effects
  - Alkali aggregate reaction
  - Delayed ettringite formation
- Distributed reinforcements effects
  - Elasto-Plasticity with linear kinematic hardening
  - Stress relaxation (with a dependence on the temperature)
  - Dowel effect
  - Matrix - distributed reinforcements sliding (method under licence(c)LMDC)

- Probabilistic scale effect based on the Weakest Link and Localization method

  Considers random distribution of tensile strength without random sampling

  Direct access to the most likely failure mode (WL2 method [42]).

- Strengh in tension and compression dependence on loading speed

  Modified CEB dynamic amplification coefficient for tensile and compressive strength

  Strenght amplification from $5.10^{-6}s^{-1}$

Interactions between phenomemena

The method used to couple the different mechanisms involved in the behaviour law of the matrix consists to work in a poro-mechanics framework [13]. Some interactions exit between the different phases presents in the pores thanks to their poro-mechanics formulation. For instance the pressure induced by a swelling reaction acts on the solid skeleton of the matrix, which in turn is damaged in tension. Concerning the reinforcements, their effects are considered through a mix law method. The different options concerning the organization between the different modules are schemed in figure 1.

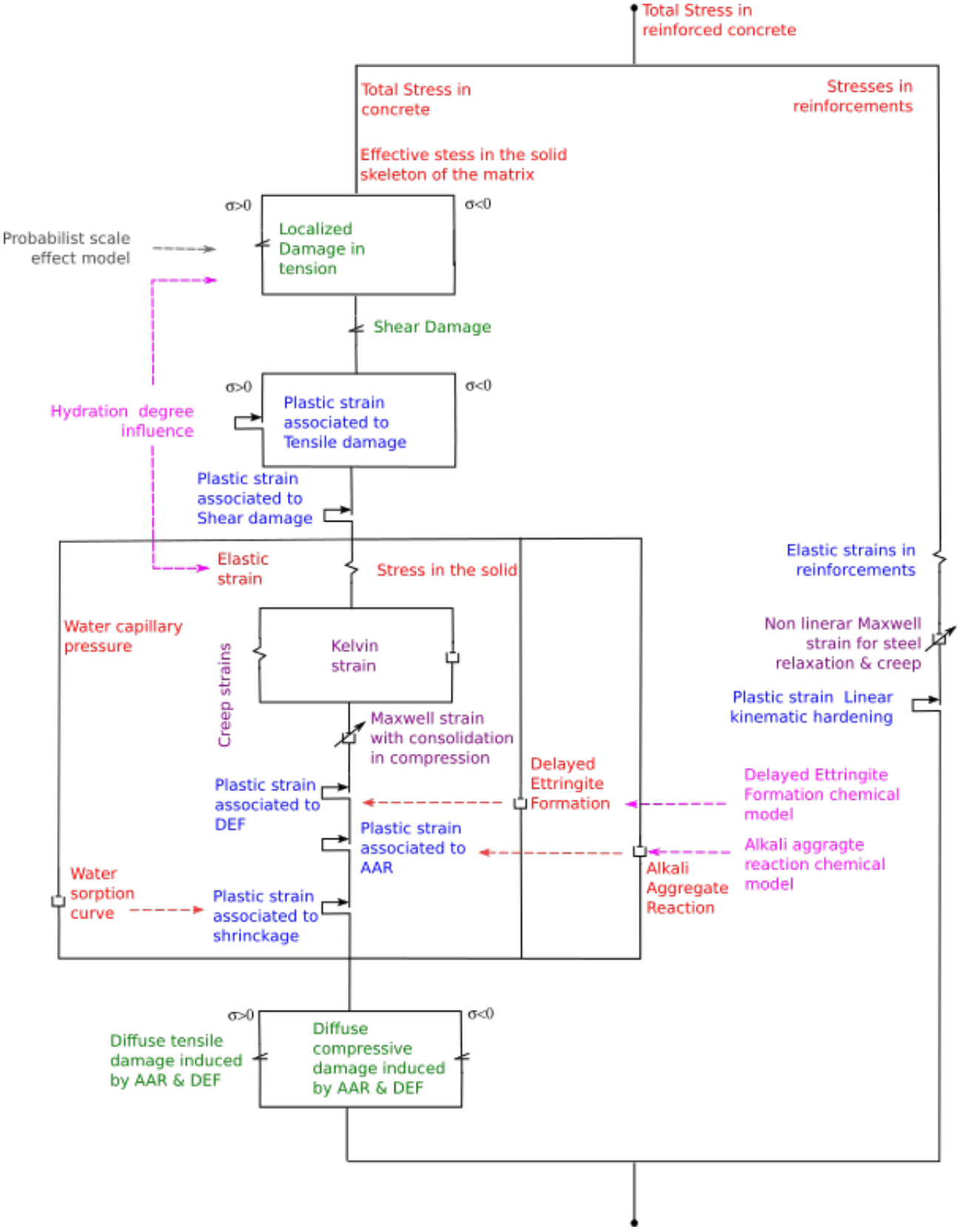

Figure 1: Global rheologic scheme

Part II

Constitutive equations

Chapter 1

Delayed strains

1.1 Basic creep

Delayed strains of solid skeleton are called basic creep strains. They can be permanent or reversible, depending on underlying phenomena. In the model, basic creep constitutive equations are always used coupled to a plastic strains model which insures the stress field compatibility with the strength criteria. Practically, the basic creep model involves two usual rheologic modules : a Kelvin solid for reversible creep and a Maxwell visco elastic fluid for permanent creep as illustrated in figures 1 and 1.1. Effects of poral pressure are considered through the poromechanics framework [44].

1.1.1 Permanent creep

Constitutive relations

Basic creep is a macroscopic consequence of nano-scale phenomena, in fact some solid phases are intrinsically viscous due to the weak inter-atomic links existing at the lowest scales. When submitted continuously to a loading, these links locally break and repair (or not) and a new geometric configuration is reached, corresponding to a delayed macroscopic strain. At the macroscopic scale, it is assumed that permanent creep velocity is proportional to the elastic strain (ε^E) as expressed in equation (1.1). This assumption is supported by experimental evidences showing that multiaxial creep can be deduced from uniaxial creep with a quasi constant

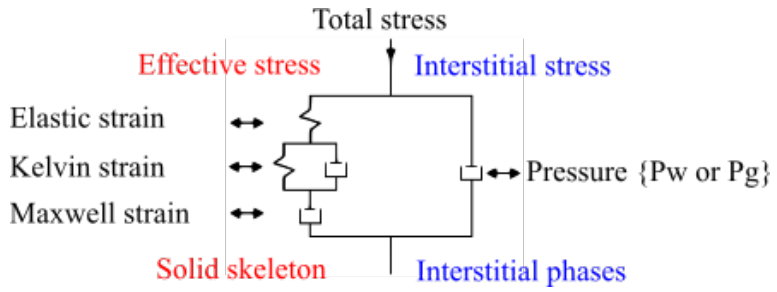

Figure 1.1: Idealized rheologic scheme for poro-mechanics creep model

Poisson ratio effect [18].

$$\frac{\partial \varepsilon_{IJ}^{M}}{\partial t} = \frac{\varepsilon_{IJ}^{E}}{\tau_{IJ}^{M}} \tag{1.1}$$

In this equation τ_{IJ}^{M} if the characteristic time for the strain component ε_{IJ}^{M} with I and J subscripts corresponding to eigen-directions of $\boldsymbol{\varepsilon}^{M}$. In this base τ_{IJ}^{M} can be assessed with equation (1.2).

$$\tau_{IJ}^{M} = \min\left(\tau_{I}^{M}, \tau_{J}^{M}\right) \tag{1.2}$$

With τ_{I}^{M} defined by equation 1.3. In fact, at nano-scale basic creep is caused by atomic link instabilities, which are themselves affected by physical conditions (temperature (T), humidity (H) and mechanical loading (M)). At upper scale (micro and meso scale) stress redistribution between viscous phases and non-viscous phases leads to consolidation (C) and damage (D). consequently the basic creep characteristic time (τ_{I}^{M}) is managed by at mean three physical conditions:

- Temperature (T),
- Humidity (H),
- Mechanical loading (M).

These three conditions influence the way how the material evolves two physical phenomena for which internal variable have to be defined and linked to the characteristic time :

- Consolidation (C),
- Damage (D).

Damage acts directly at macro level to amplify elastic strain , as usually admitted in damage mechanics theory [21][26].In the model damage Variable D^{C} and D^{T} used in (3.1) consider respectively creep damage and thermal damage. Consolidation is considered using a consolidation function C_{I}^{C} affecting characteristic time :

$$\tau_{I}^{M} = \tau_{ref}^{M} C_{I}^{C} \tag{1.3}$$

With τ_{ref}^{M} a reference characteristic time, used as fitting parameter in reference condition (high humidity, reference temperature, without initial creep strain). Permanent creep strain origins take place in viscous material phases of solid skeleton. But solid skeleton contains also non viscous grains, and microscopic arrangements of viscous and non viscous phases is generally aleatory. As viscous strains come along with strains of non viscous grains, a local heterogeneity of stress and strain fields appears. The macroscopic consequence of this heterogeneity is that non-viscous phases oppose to viscous strains of viscous ones. At the beginning viscous strains are relatively easy, but the number of non-viscous inclusions hampering viscous strain increases with the creep deformation. If non-viscous inclusions are only elastically perturbed the creep is reversible (see 1.1.2), but if non-viscous inclusions are embedded in a viscous matrix, a permanent creep appears. The consolidation function is proposed to model these phenomena in a simplify way at the macroscopic scale, the consolidation function C_{I}^{C} was initially proposed in an isotropic form in [39] and improved in [38]. The current version uses an an-isotropic

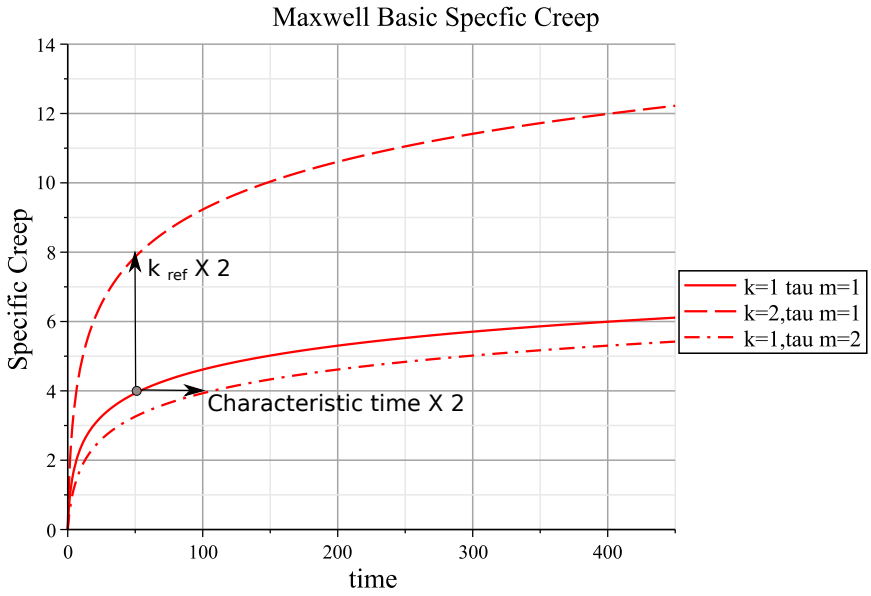

Figure 1.2: Specific Creep from Maxwell module, parametric study with k_{ref} and characteristic time τ^M_{ref}

version of consolidation coefficient which allows to consider different consolidation velocity in the different loading directions. Its expression is given by (1.4).

$$C^C_I = \frac{1}{k} \exp\left(\frac{1}{k}\left(\frac{\varepsilon^M_I}{\varepsilon^E_{II}}\right)^+\right) \tag{1.4}$$

The positive part $()^+$ means the consolidation coefficient cannot be lesser than $1/k^M$. ε^E_{II} is the elastic strain in direction I, k^M is the creep coefficient for the current temperature and loading :

$$k = k_{ref} C^T C^H C^M \tag{1.5}$$

with k_{ref} the creep coefficient defined as the ratio a characteristic strain of creep and a reference elastic strain corresponding to a standard loading.

$$k_{ref} = \frac{\varepsilon^M_{ref}}{\varepsilon^E_{ref}} \tag{1.6}$$

with ε^M_{ref} a fitting parameter called *reference creep potential* ; ε^E_{ref} a reference elastic strain corresponding to loading for which ε^M_{ref} and τ^M_{ref} are fitted. This reference elastic strain is currently fixed arbitrary to the third of compression strength ($R^C_{ref}/3$). C^T considers influence of temperature on creep potential, C^H the influence of humidity, and C^M the non linear effect of mechanical loading.

Water Effect on basic creep

Some solid cohesion forces are sensitive to the water saturation degree as explained in 1.2. In the model a linear dependence is used :

$$C^H = S_r \tag{1.7}$$

With $S_r = \phi_w/\phi$ the water saturation rate of porosity (ϕ_w the water content and ϕ the porosity).

Temperature effects on basic creep

Temperature has two effects on basic creep; on one hand it modifies intrinsic viscosity of viscous phases embedding water, due to the dependence of water viscosity to temperature, and on the other hand provokes differential dilation between phases, this last can increase creep potential releasing viscous phases, an cause thermal damage.

$$C^T = C_w^T C_p^T \tag{1.8}$$

The effect of temperature on water viscosity is taken equal to the water viscosity dependence to temperature, it is an Arrhenius law independent of material composition. In (1.9) $E_w^a \approx 17000 J/mol$ the activation energy of water viscosity T_{ref} the reference temperature for which the characteristic time τ_{ref}^M is measured, and $R = 8.31 J/mol/K$ the gaz constant.

$$C_w^T = \exp\left(-\frac{E_w^a}{R}\left(\frac{1}{T} - \frac{1}{T_{ref}}\right)\right) \tag{1.9}$$

$$C_p^T = \begin{cases} \exp\left(-\dfrac{E_p^a}{R}\left(\dfrac{1}{T} - \dfrac{1}{T_{thr}}\right)\right) & \text{if } T > T_{thr} \\ 1 & \text{if } T \leqslant T_{thr} \end{cases} \tag{1.10}$$

C_p^T function parameters depend on material composition through two fitting parameters : $E_p^a \approx 25000 J/mol$ which is is a fitting constant and $T_{thr} \approx 45°\text{C}$ the threshold temperature from which thermal damage appears and modifies the creep potential [25].

Mechanical loading effect on basic creep

The Mechanical loading coefficient C^M considers the possible non linear dependence of creep potential on mechanical loading level. So, C^C starts from 1 for unloading material and diverges if loading level reaches a critical value provoking tertiary creep. As it is assumed tertiary creep occurs only in case of deviatoric loading, C^C depends only on the loading level through an equivalent shear stress τ^{DP} :

$$C^M = \frac{\tilde{\tau}_{cr}^{DP}}{\tilde{\tau}_{cr}^{DP} - \tilde{\tau}^{DP}} \tag{1.11}$$

A Drucker Prager formulation [17] is chosen for τ^{DP} to consider benefits of triaxial confinement to reduce deviatoric creep. In fact $\tilde{\tau}^{DP}$ is a function of two first stress tensor invariants. (1.12), and $\tilde{\tau}_{cr}^{DP}$ the Drucker Prager critical stress leading to tertiary creep.

$$\tilde{\tau}^{DP} = \sqrt{\frac{\tilde{\sigma}^d : \tilde{\sigma}^d}{2}} + \delta \frac{\text{Tr}\left(\tilde{\sigma}\right)}{3} \tag{1.12}$$

δ is the confinement effect coefficient which takes into account benefits of hydro-static pressure on shear strength. For some material it depends on water saturation rate, but this option is not implemented in the current version. The critical stress can be linked to the corresponding uniaxial critical stress intensity σ_{cr}, the relation implies the confinement coefficient δ and ans assume the uniaxial critical stress is a compression.

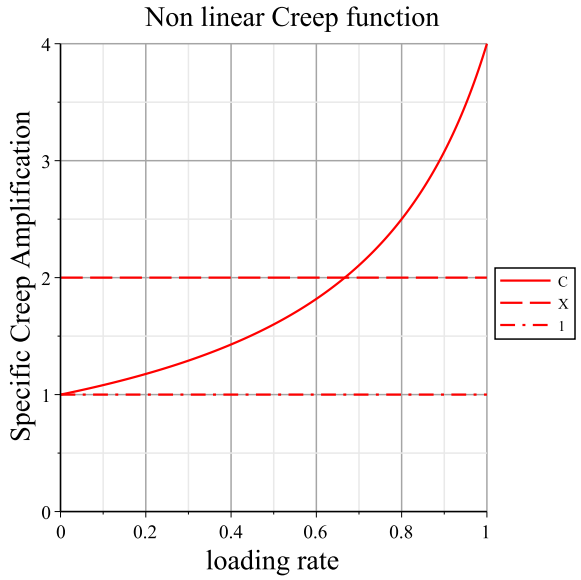

Figure 1.3: Specific creep amplification versus loading rate (red curve), amplification at 66%Rc (blue dot line X) and unit (dash line 1)

$$\tilde{\tau}_{cr}^{DP} = \frac{\tilde{\sigma}_{cr}}{\sqrt{3}}\left(1 - \frac{\delta}{\sqrt{3}}\right) \tag{1.13}$$

In the model $\tilde{\sigma}_{cr}$ is computed from a non linear amplification coefficient χ^M, supplied by the user, and corresponding to the non-linearity of creep under an applied compression stress of $66\%R_c$. With this definition the link between χ^M and $\tilde{\sigma}_{cr}$ is :

$$\tilde{\sigma}_{cr} = \frac{2}{3}\left(\frac{\chi^M}{\chi^M - 1}\right)\tilde{R}_c \tag{1.14}$$

The evolution of basic specific creep non linear amplification function is illustrated in figure 1.3.

1.1.2 Reversible creep

Constitutive relations

Reversible creep is modelled thanks to Kelvin module, in which stress is replaced by a a reduced elastic strain corresponding to the final strain of Kelvin module.

$$\frac{\partial \varepsilon_{ij}^K}{\partial t} = \frac{1}{\tau^K}\left(\frac{\varepsilon_{ij}^E}{\psi^K} - \varepsilon_{ij}^K\right) \tag{1.15}$$

Reversible creep, like permanent creep depends on temperature and water content. The same coefficients, C_w^T (equation 1.9) and C^W (equation 1.7), than for permanent creep are used.

$$\tau^K = \tau_{ref}^K C^W C_w^T \tag{1.16}$$

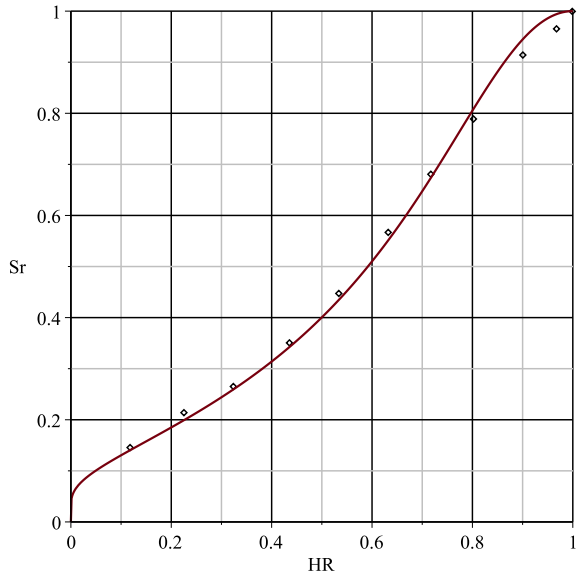

Figure 1.4: Isotherm *(dots: experiments from [3], line: Van Genuchten's equation with* $M_{sh} = 44MPa$ *and* $m_{vg} = 0.5$*)*

1.2 Shrinkage and drying creep

Water has complex effects in porous media. It can react with solid skeleton, be adsorbed on porous walls, and exerts capillary forces on solid skeleton. In some materials, such as clay or concrete, water molecules are present in nanoscopic material inter-layers causing attractive or repulsive forces according to their environmental conditions (mechanical loading, temperature...). These effects have several macroscopic consequences. Among other, delayed strains depend on the thermo-mechanical state of water. To model the most important visible consequences of water solid interactions it is convenient resorting to the capillary pressure theory in the context of poro-mechanics (Biot theory extended to non saturated media by Coussy).

1.2.1 Water capillary pressure

The capillary pressure can be modeled using a two parameters water retention curve equation called *Van-Genuchten model*. This equation provides the capillary pressure (P_c) as a function of saturation rate (S_r). If gas pressure is neglected relatively to water pressure (P_w), water pressure can be directly expressed as a function of water saturation rate (1.17) as illustrated in figure 1.4 page 18.

$$P_w = M_{sh}\left(1 - S_r^{\left(-\frac{1}{m_{vg}}\right)}\right)^{(1-m_{vg})} \tag{1.17}$$

The water retention curve given by (1.17) is modified by temperature. At high temperature, for a given relative humidity, the saturation rate Sr decreases as observed in [34].The dependence to the temperature is modelled changing the Van Genuchten equation parameter's M_{sh}. (1.18).

$$M_{sh} = M_{sh}^{ref} \exp\left(-\frac{T - T_{ref}}{T_k^{vg} - T_{ref}}\right) \tag{1.18}$$

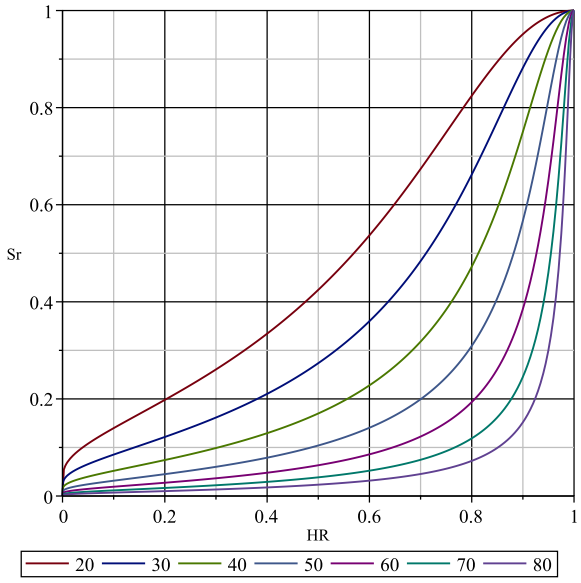

Figure 1.5: Isotherms at different temperatures (for $M_{sh}^{ref} = 41MPa$, $m_{vg} = 0.5$, $T_k^{vg} = 40$C, $T_{ref} = 20$C)

In (1.18),M_{sh}^{ref} is the Van Genuchten parameter M_{sh} at temperature T_{ref}, T is the current temperature, and $T_k^{vg} \approx 40$C a fitting parameter. An example of temperature effect on a water retention curve is given in figure 1.5.

1.2.2 Interactions between water and solid

Shrinkage is induced by solid-water interactions. Tension forces at interfaces between *liquid water* and *gas* acts on *solid skeleton* to contract it, but the efficiency how the pressure acts depends on the stress state σ applied on material. In fact as explained in [39, 38], solid skeleton can be damaged by differential shrinkage between solid grains more or less sensitive to water content variation (specially aggregates and paste in concrete). If this damage occurs, it limits the capillary pressure transmission from paste to other phases and the macroscopic effect of paste shrinkage is reduced. On the contrary, if a compression stress is applied in a direction, damage induced by differential shrinkage between paste and aggregate is avoided and capillary pressure are better transmitted. To consider this non linear interaction between solid skeleton and water effects during drying or humidification, the cracking induced by the cpaillary forces is modeled as illustrated in the global rheologic scheme 1.In tension or weak compression the matrix cracks and the caipllary effect is not integrally transmitted at upper scales while under high compression, the pressure effect is balanced by the compression and the abscence of cracking leads to a better transmission of capillary forces from micro structures to macro-scale [40].

1.3 Transient thermal creep

Transient thermal creep is observed only if material is loaded in compression just before or during heating [4]. According to Cagnon et al.[8], it depends also on the consolidation state of material, and it is proportional to the heating rate. Its modeling is under clarification in the PhD of F.Manzoni (to be published sept 2019).

Chapter 2

Plastic strains

Several plastic criteria are used in the model, each of them manages the evolution of an inelastic strain. Most of these criteria are written in terms of *total undamaged stresses*(2.1), itself obtained by time integration of total stresses increments (2.2).

$$\tilde{\sigma}_{ij} = \int_0^t \mathrm{d}\tilde{\sigma}_{ij} \tag{2.1}$$

The total undamaged stress increment depends on effective stress increment $\mathrm{d}\tilde{\sigma}'_{ij}$ which is relative to the solid skeleton behavior, and $\mathrm{d}\left(b_g p_g + b_w p_w\right)$ relative to the porous pressures, $\mathrm{d}\left(b_g p_g\right)$ for the gel pressure and $\mathrm{d}\left(b_w p_w\right)$ for the hydric effects.

$$\mathrm{d}\tilde{\sigma}_{ij} = \mathrm{d}\tilde{\sigma}'_{ij} - \delta_{ij}\mathrm{d}\left(b_g p_g + b_w p_w\right) \tag{2.2}$$

In (2.2), $\tilde{\sigma}'_{ij}$ is the effective stress in the undamaged part of material matrix, directly linked to the elastic strain thank to the material stiffness S_{ijkl}:

$$\mathrm{d}\tilde{\sigma}'_{ij} = S_{ijkl} : \mathrm{d}\varepsilon^E_{kl} \tag{2.3}$$

In (2.1) δ_{ij} is the Kronecker symbol used to consider internal pressure effects are equivalent to isotropic stresses. b_g and p_g are respectively the biot coefficent and pressure associted to ISR. b_w and p_w are the Biot coefficent and pressure for hydric effects. In tension three orthogonal Rankine criteria, sometimes called principal stress criteria as in [14], are used to limit the undamaged total stress(2.1) to $\tilde{R}_t$. When needed,the criteria have to be able to rotate to consider non radial loading pass. Plastic strains in tension are used to represent crack opening, but if a sufficient compression stress if applied after a damage in tension, cracks can re-closed. On purpose, and as suggested by Jefferson [20], re-closure plastic criteria can be used to model re-closure. In the present model three principal stress criteria are also used to manage independently the re-closure of the three main cracks generated in tension. In shear and compression a Drucker Prager [17] criterion is used, it is implemented in a non standard way (non associated flow) to consider possible material dilatancy. If material porosity is subjected to a pore pressure exceeding the solid skeleton tensile strength, inelastic strains appears, they are managed by three other plastic criteria written in terms of principal stresses in solid skeleton. Therefore, the model considers ten plastic criteria:

- Three for cracking in direct tension (Rankine criteria i.e Principal positive stresses) or for macro-crack re-closure (Principal negatives stresses)

- Three for solid skeleton cracking under pore over pressure induced by alkali reaction (AAR)
- Three for solid skeleton cracking under pore over pressure induced by delayed ettringite (DEF)
- Three for solid skeleton cracking under capillary pressure of free water (with possibility of micro crack reclosing)
- One for shear cracking (Drucker Prager with non associated flow), this is this last criterion which considers implicitly the failure in compression.

These 13 plastic criteria manage 5 plastic strains tensors :

- One for plastic strain in tension, managed by the first plastic criteria
- One for inelastic strain induced by AAR
- One for inelastic strain induced by DEF
- One for inelastic strain induced by the Water
- One for shear and compression

The specificity of the model consists in its ability to manage together the two types of creep strains (reversible and permanent) and the plastic criteria.

2.1 Plastic criteria

The Rankine criteria f^t, re-closure criteria f^r, and Over pressure criteria f^g are defined in the principal base of undamaged stresses tensor $\{\tilde{\sigma}_I, \tilde{\sigma}_{II}, \tilde{\sigma}_{III}\}$. Therefore, the orthotropic tensile criteria can be expressed as follows :

$$f_I^t = \tilde{\sigma}_I - \tilde{R}_I^t \text{ with } I \in [I, II, II] \tag{2.4}$$

$\tilde{R}_I^t$ the effective tensile strength in a principal direction of stress. If a tensile plastic strain occurs, and if an unloading occurs later, the following re-closure criteria can be reached, they lead to a reduction of tensile plastic strains :

$$f_I^r = \begin{cases} (-\tilde{\sigma}_I) - \tilde{R}_I^r \text{ with } I \in [I, II, II] & \text{if } \varepsilon_I^{pl,t} > 0 \\ 0 & \text{if } \varepsilon_I^{pl,t} \leqslant 0 \end{cases} \tag{2.5}$$

With $\tilde{R}_I^r$ the stress needed to re-close a tensile crack, and $\varepsilon_I^{pl,t}$ the plastic strain induced by Rankine criteria in tension (2.4). In criteria (2.4) or (2.5), the stress $\tilde{\sigma}_I^{eq}$ involved is associated to external loading, so as considered in the section dedicated to damage, the plastic strain associated to Rankine and Re-closure criteria correspond to localized cracks, but diffuses cracks can also occur in case of over pressure induced by AAR, DEF or WATER in material porosity. This possibility is considered through the over-pressure criteria which are obtained replacing $\tilde{\sigma}_I$ by $\tilde{\sigma}_I^{eq}$ in (2.6):

$$f_I^g = \underbrace{C^g\ p^g + \min(\tilde{\sigma}_I, 0)}_{\tilde{\sigma}_I^{eq}} - \tilde{R}_I^t \text{ with } I \in [I, II, II] \tag{2.6}$$

With p^g the pressure, and C^g the stress concentration factor associated to this pressure. Thank to this coefficient C^g, users have the possibility to control the ability for pressure to create cracking and plastic strains. In fact, if $C^g = 0$ and $b^g \neq 0$ the gel acts only through the linear poro-mechanical effect, while, on the contrary, if $b^g = 0$ and $C^g \neq 0$, the gel creates cracking and plastic strains without poro-mechanical effects. Of course all other intermediate cases can be envisioned, provided that $b^g \leqslant 1$. From a practical point of view, the plastic swelling associated to these cracks becomes anisotropic in presence of anisotropic compressive loading.

Another cause of diffuse cracking leading to plastic strain is the propagation of micro-cracks induced by shear stresses. This cracking phenomenon is sensible to hydrostatic pressure which improves the shear strength. To model this last cracking possibility a Drucker Prager criterion is used.

$$f^{DP} = \left(\sqrt{\frac{\tilde{\sigma}^d_{ij} : \tilde{\sigma}^d_{ij}}{2}} + \delta \frac{\mathrm{Tr}\left(\tilde{\sigma}_{ii}\right)}{3} \right) - \tilde{R}^c \left(\frac{1}{\sqrt{3}} - \frac{\delta}{3} \right) \tag{2.7}$$

$\tilde{R}^c$ the compressive strength, δ the Drucker Prager confinement coefficient, $\tilde{\sigma}^d$ the diviatoric components of stress tensor,$\mathrm{Tr}\left(\tilde{\sigma}\right)$ its trace. To manage interaction between Drucker Prager and Rankine criteria the following conditions are added:

- First, the initial threshold of compression hardening ($\tilde{R}^c_0$) is chosen such as the tri-tension state reaches earlier the Rankine criteria than the Drucker Prager criterion :

$$\tilde{R}^c_0 \geqslant \tilde{R}_t \frac{3\delta}{\sqrt{3} - \delta} \tag{2.8}$$

- Secondly, a uniaxial tension in any main direction must reach the Rankine criterion before the Drucker Prager one.

$$\tilde{R}^c_0 \geqslant \tilde{R}_t \frac{\sqrt{3} + \delta}{\sqrt{3} - \delta} \tag{2.9}$$

With these additive conditions,Drucker Prager criterion cannot be reached by a tri-tension stress state. A multidimensional plot of Drucker Prager and Rankine criteria is given in figure 2.1, this figure allows to see the Rankine criteria are reached first in tri-tension and uni-directional tension. The Drucker-Prager criterion is active only if at least one principal direction is a compression.

2.2 Plastic flow

2.2.1 Consistence condition

Anelastic strains result from a Kuhn Tucker problem with the objective (2.10).

$$f^i \leqslant 0 \ \forall i \in [1...N] \tag{2.10}$$

In (2.10) $i = 1 \rightarrow N$ stands for each criterion ($N \leq 13$)). As $f^i(\tilde{\sigma}) \leqslant 0$ are convex domains, as illustrated in figure 2.1 in the principal stress base, it is possible to find Lagrange multiplicators λ^i satisfying the consistence conditions (2.11).

$$\forall i \in [1..N] \ / \ f^i > 0 \ \rightarrow f^i + \sum_{j=1}^{N} \mathrm{d}\lambda^j \frac{\partial f^i}{\partial \lambda^j} = 0 \tag{2.11}$$

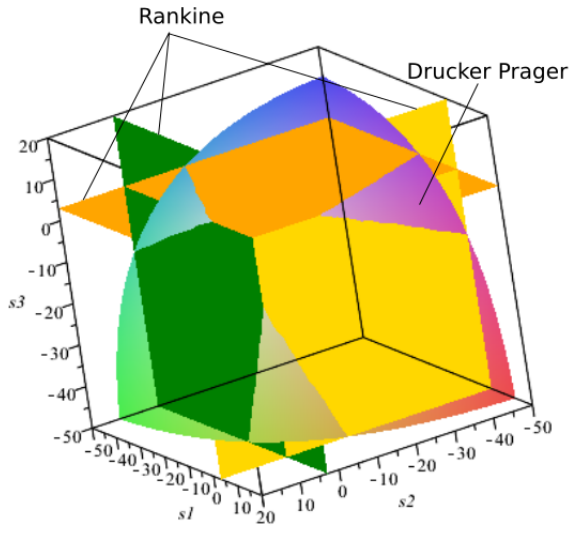

Figure 2.1: Plastic criteria in principal stresses base s_1, s_2, s_3, ($R_t = 3MPa$, $R_c = 30MPa$, $\delta = 1$)

With N the number of criteria activated by a total strain increment starting from a previous admissible stress state, and computed assuming none plastic flow during the first elasto-plastic tentative (analogous to the elastic predictor step in elasto-plastivity). Solving (2.11) consists to find Lagrange multiplicator increments $\mathrm{d}\lambda^j$. The algorithm used is based on a *return mapping* one [30]. As some criteria f^j use directly a pressure (P) in their expression (2.6), the general form for the variation of f^j is :

$$\frac{\partial f^i}{\partial \lambda^j} = \frac{\partial f^i}{\partial \tilde{\sigma}_{kl}} \frac{\partial \tilde{\sigma}_{kl}}{\partial \lambda^j} + \sum_g \frac{\partial f^i}{\partial p^g} \frac{\partial p^g}{\partial \lambda^j} + \frac{\partial f^i}{\partial \tilde{R}^i} \frac{\partial \tilde{R}^i}{\partial \lambda^j} \tag{2.12}$$

with $g \in [AAR, DEF, Water]$.

2.2.2 Plastic strain increment direction

For each active criterion, the plastic strain increment is assumed to derive from a convex yield function F^i such as :

$$\mathrm{d}\varepsilon^{pl,j}_{mn} = \mathrm{d}\lambda_j \frac{\partial F^j}{\tilde{\sigma}_{mn}} \tag{2.13}$$

For Rankine criteria (tension or reclosure for external loading or its combination with stress induced by a pressure in the porosity), the plasticity is associated:

$$F^i = f^i \text{ if } i \leqslant 12 \tag{2.14}$$

For the shear criterion (Drucker Prager), a non associated Yield function is used to control the dilatancy:

$$F^{DP} = \sqrt{\frac{\tilde{\sigma}^d_{ij} : \tilde{\sigma}^d_{ij}}{2}} + \beta \frac{\mathrm{Tr}\,(\tilde{\sigma}_{ii})}{3} \tag{2.15}$$

With β the dilatancy coefficient ($\beta = 0$ induces a plastic flow without dilatancy).

2.2.3 Plasticity and Creep Coupling

If creep is considered, the effective stresses and the pressures depend also on the Kelvin and Maxwell strains, so these strains evolve during the return mapping procedure, and consequently the criteria function evolution depend also on their increments. The dependence of plastic criteria on creep strains is given by (2.16).

$$\left\{ \begin{array}{l} \dfrac{\partial f^i}{\partial \varepsilon^K_{mn}} = \dfrac{\partial f^i}{\partial \tilde{\sigma}'_{kl}} \dfrac{\partial \tilde{\sigma}'_{kl}}{\partial \varepsilon^K_{mn}} + \dfrac{\partial f^i}{\partial p^g} \dfrac{\partial p^g}{\partial \varepsilon^K_{mn}} \\ \dfrac{\partial f^i}{\partial \varepsilon^M_{mn}} = \dfrac{\partial f^i}{\partial \tilde{\sigma}'_{kl}} \dfrac{\partial \tilde{\sigma}'_{kl}}{\partial \varepsilon^M_{mn}} + \dfrac{\partial f^i}{\partial p^g} \dfrac{\partial p^g}{\partial \varepsilon^M_{mn}} \end{array} \right. \tag{2.16}$$

The dependence can be expressed using the evolution of effective stress versus elastic strain (2.3), in which, during the return mapping at constant total strain, the elastic strain increment can be replaced by the sum of inelastic strains increments:

$$\mathrm{d}\varepsilon^E_{mn} = -\left(\sum_j \mathrm{d}\varepsilon^{pl,j}_{mn} + \mathrm{d}\varepsilon^K_{mn} + \mathrm{d}\varepsilon^M_{mn} \right) \tag{2.17}$$

The effective stresses variations are deduced using the stiffness matrix components S_{klmn}:

$$\left\{ \begin{array}{l} \dfrac{\partial \tilde{\sigma}'_{kl}}{\partial \lambda^j} = -S_{klmn} \dfrac{\partial \varepsilon^{pl,j}_{mn}}{\partial \lambda^j} = -S_{klmn} \dfrac{\partial F^j}{\partial \tilde{\sigma}_{mn}} \\ \dfrac{\partial \tilde{\sigma}'_{kl}}{\partial \varepsilon^K_{mn}} = \dfrac{\partial \tilde{\sigma}'_{kl}}{\partial \varepsilon^M_{mn}} = -S_{klmn} \end{array} \right. \tag{2.18}$$

As anelastic strains affect also the pressures though the term $(b^g p^g)$, the total stress variation induced by a plastic strain increment becomes:

$$\left\{ \begin{array}{l} \dfrac{\partial \tilde{\sigma}_{kl}}{\partial \lambda^j} = -\left(S_{klmn} + \delta_{kl}\delta_{mn} \dfrac{\partial b^g p^g}{\partial \varepsilon^{pl,j}_{mn}} \right) \dfrac{\partial F^j}{\partial \tilde{\sigma}_{mn}} \\ \dfrac{\partial \tilde{\sigma}_{kl}}{\partial \varepsilon^K_{mn}} = -S_{klmn} + \delta_{kl}\delta_{mn} \dfrac{\partial b^g p^g}{\partial \varepsilon^K_{mn}} \\ \dfrac{\partial \tilde{\sigma}_{kl}}{\partial \varepsilon^M_{mn}} = -S_{klmn} + \delta_{kl}\delta_{mn} \dfrac{\partial b^g p^g}{\partial \varepsilon^M_{mn}} \end{array} \right. \tag{2.19}$$

The Kronecker symbol ($\delta_{mn} = 1$ if $(m = n)$) is used to consider that the pressure affects only normal stresses. Coupling between creep strains and plastic strains depends on the numerical method chosen to solve the creep problem. If the general method used for temporal integration is a semi-implicit scheme (θ method for instance), the elastic strain involved in the creep increment assessment is a mix between its values at beginning and the end of the time step:

$$\left\{ \begin{array}{l} \mathrm{d}\varepsilon^K_{mn} = \dfrac{\mathrm{dt}}{\tau^K} \left[\left(\dfrac{\varepsilon^E_{mn}}{\psi^K} - \varepsilon^K_{mn} \right)_t (1-\theta) + \theta \left(\dfrac{\varepsilon^E_{mn}}{\psi^K} - \varepsilon^K_{mn} \right)_{t+dt} \right] \\ \mathrm{d}\varepsilon^M_{mn} = \left(\dfrac{\mathrm{dt}}{\tau^M_{mn}} \varepsilon^M_{mn} \right)_t (1-\theta) + \theta \left(\dfrac{\mathrm{dt}}{\tau^M_{mn}} \varepsilon^M_{mn} \right)_{t+dt} \end{array} \right. \tag{2.20}$$

As the return mapping is applied after visco-elastic prediction, only the variation of ε^E_{mn} at the end of the step time is considered. The equation's set to be solved for the return mapping is

deduced (2.21). It allows to assess simultaneously the creep strain corrections $\mathrm{d}\varepsilon^K_{mn}$ and $\mathrm{d}\varepsilon^M_{mn}$, and the plastic multiplicators $\mathrm{d}\lambda^j$:

$$\begin{cases} \mathrm{d}\varepsilon^K_{mn}\left(1+\dfrac{\theta \mathrm{dt}}{\tau^K}\left(1+\dfrac{1}{\psi^K}\right)\right)+\dfrac{\theta \mathrm{dt}}{\psi^K\tau^K}\left(\mathrm{d}\varepsilon^M_{mn}+\mathrm{d}\lambda^j\dfrac{\partial F^j}{\partial\sigma_{mn}}\right)=0 \\ \mathrm{d}\varepsilon^M_{mn}\left(1+\dfrac{\theta \mathrm{dt}}{\tau^M_{mn}}\right)+\dfrac{\theta \mathrm{dt}}{\tau^M_{mn}}\left(\mathrm{d}\varepsilon^K_{mn}+\mathrm{d}\lambda^j\dfrac{\partial F^j}{\partial\sigma_{mn}}\right)=0 \\ \mathrm{d}\varepsilon^K_{mn}\dfrac{\partial f^i}{\partial\varepsilon^K_{mn}}+\mathrm{d}\varepsilon^M_{mn}\dfrac{\partial f^i}{\partial\varepsilon^K_{mn}}+\mathrm{d}\lambda^j\dfrac{\partial f^i}{\partial\varepsilon^{pl,j}_{mn}}\dfrac{\partial F^j}{\partial\sigma_{mn}}+f^i=0 \end{cases} \tag{2.21}$$

Once the plastic multiplicators are computed the plastic strain increment can be assessed using (2.13). The creep strains have also to be actualized to consider their variations during the return on yield surfaces.

2.3 Effective strength hardening laws

Plasticity is used to limit effective stress $\tilde{\sigma}^{eq}$. During damage process if a residual undamaged material sub-zone subsists, it is because its effective strength is greater then the material already damaged. So, a positive or null hardening is chosen to model each effective strength evolution versus plastic strain. Note this choice is not in contradiction with a softening behaviour of concrete, it means simply that softening is not due to the plasticity but to the damage induced by the plasticity. The coupling between plasticity and damage will be treated in the next section.

$$\frac{\partial \tilde{R}^t_I}{\partial \lambda^{\tilde{R}^t_I}} = H^t \geq 0 \tag{2.22}$$

In compression a non linear hardening function $H^c(\varepsilon^{pl,c,eq})$ is defined such as the global uni-axial stress-strain response remains parabolic until the compression strength $\tilde{R}^c$ is reached.

$$\frac{\partial \tilde{R}^c}{\partial \lambda^{\tilde{R}^c}} = H^c(\varepsilon^{pl,c,eq}) \geq 0 \tag{2.23}$$

$\varepsilon^{pl,c,eq}$ is the equivalent plastic strain defined as follows :

$$\varepsilon^{pl,c,eq} = \sqrt{\frac{2}{3}}\int_0^t \sqrt{\mathrm{d}\varepsilon^{pl,c}_{mn}\mathrm{d}\varepsilon^{pl,c}_{mn}} \tag{2.24}$$

and the hardening function is build such as the uni-axial pre-pick behavior law is:

$$\tilde{\sigma} = \tilde{R}^c_0 + \left(\tilde{R}^c - \tilde{R}^c_0\right)\left(1-\left(1-\frac{\varepsilon-\varepsilon_0}{\varepsilon^c-\varepsilon^0}\right)^2\right) \tag{2.25}$$

After the pick, a quasi null hardening is used as illustrated in 2.2. For over pressure criteria, a constant and positive hardening H^g is used to avoid unstable bifurcation of micro-cracks induced by over pressures. In fact, in case of isotropic loading, if none hardening would be used, the crack propagation would occur arbitrarily in a given main direction and would continue in this one only, leading to an arbitrary an-isotropic swelling.

$$\frac{\partial \tilde{R}^g_I}{\partial \lambda^{\tilde{R}^g_I}} = H^g \geq 0 \tag{2.26}$$

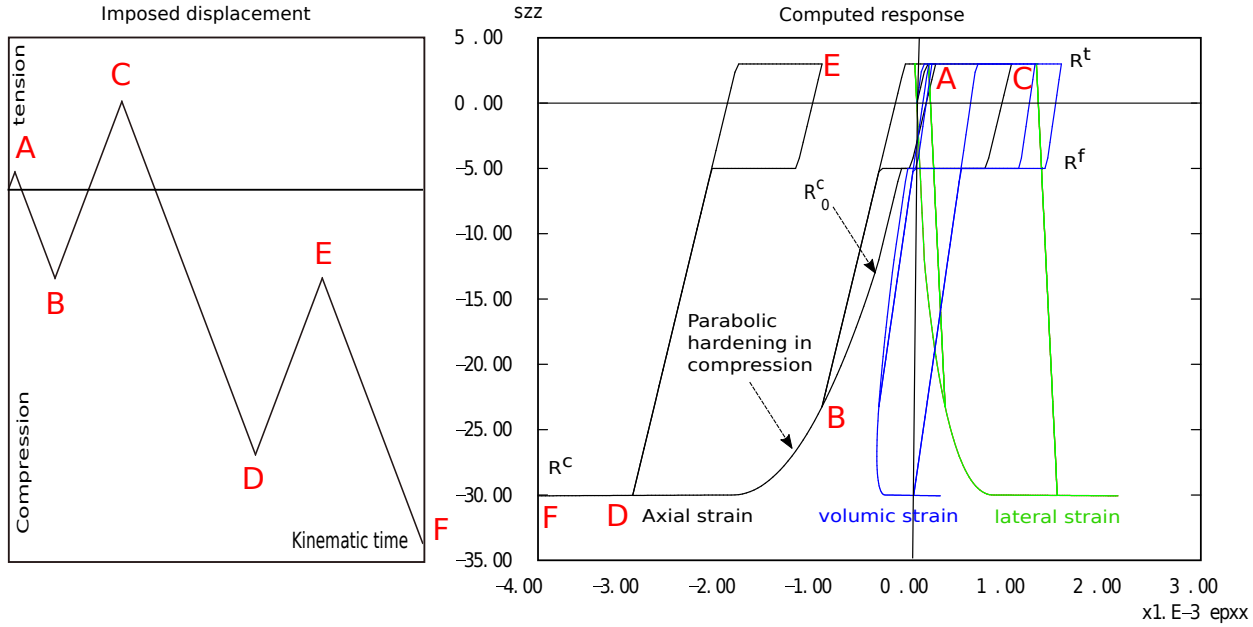

Figure 2.2: Uniaxial tension-compression cycles without damage, ($R_t = 3MPa$, $R^f = 5MPa$, $R_c = 30MPa$, $\delta = 1$, $\beta = 0.15$). Left figure : imposed axial strain versus time, left figure: effective stress computed by the model (axial stress versus axial strain (black), radial strain (green), volume strain (blue)

For crack reclosure, a positive or null hardening is used to represent effective stress able to crush crack edge roughness.

$$\frac{\partial \tilde{R}_I^f}{\partial \lambda^{\tilde{R}_I^f}} \geq 0 \tag{2.27}$$

If used together with the damage theory, this effective stress is affected by an integrity variable $R^r = 1 - D^r$ which considers the roughness density decrease versus crack opening. As this integrity variable is not yet applied in 2.2, the crack reclosure stress R^f appears to be constant (bacause in this example $H^{=}0$), in fact it is the *effective* reclosure crack, notyet the apparent one.

2.4 Numerical implementation of creep and multi-criteria coupling

2.4.1 Treatment of interaction between criteria

For some criteria, like the ones concerning diffuse cracking, the external stresses used in the criteria to balance the pressure effects can be overestimated before all the other criteria (Drucker Prager or Rankine) are verified, that is the reason why the positive stresses used in these criteria are limited to positive or null conventional values. The current values used are zero, so that only the negative part of un-damaged stresses are considered to mitigate swelling due to the pressure of AAR or DEF.

2.4.2 Hierarchical resolution of multi-criteria plasticity

Solving multi-criteria plasticity can present some difficulties when several Rankine criteria and Drucker Prager one are active simultaneously. In fact a classical radial return mapping algorithm can lead to an overestimation of some plastic strains to the detriment of other ones. For instance when a great strain increment leads to exceed simultaneously the Rankine and the Drucker Prager criteria several paths allow to return onto the yield surfaces. That is the reason why a hierarchical method is used to consider progressively the coupling between the different plastic flows: First the Rankine criteria are solved for the diffuse cracking alone, then the criteria for external loading are verified.During this second stage of solving, if a localized crack re-closure occurs, the verification of the corresponding criterion is proprietary.

Chapter 3

Damages

As suggested by Kachanov [21] or Lemaitre and Chaboche [26], damage origin takes place in the creation of cavities in the material, which come along with plastic phenomena. For geo-material such as rocks and concrete, the damage theory is usually used until failure. Therefore, it includes not only the stage of voids nucleation, as in the original theory of Kachanov, but also the void coalescence until macro-crack occurrence. Consequently damage models such as Mazars [28], Laborderie [23], Pijaudier-Cabot [31] [10] base their criteria on strain extensions which is supposed representative of crack opening. In the present model, damage is also based on extension phenomena, but the link with the void nuclation is assumed driven only by an-elastic strains. In addition to creep and thermal damage, one damage is associated to each positive plastic strain type. Consequently several damage families coexist in the model:

- As tensile damage becomes strongly anisotropic during localization process, in the post peak phase of the behaviour law, two types of tensile damages are differentiated in the model, an isotropic one before tensile peak (D_0^t in (3.1)), based on effective stress evolution, and an orthotropic one after the peak. Post peak localized damage in direct tension (D_{ijkl}^t in (3.1)) is associated to Rankine plastic strains, so it is computed in each main principal direction of plastic strain in tension,it is an orthotropic damage able to rotate according to the plastic strain tensor evolution [36, 37].

- Damages induced by AAR, DEF and capillary pressure, also computed in each principal direction of plastic strain tensor induced by over pressure of AAR, and able to rotate with it [41][9]. As shown in [9], effects of AAR cracks are different on tensile and compressive stresses, due to the fact that compressive stresses re-close some AAR micro-cracks. So, this damage is split in two parts, D_{ijkl}^{tg} and D_{ijkl}^{cg} in (3.1) (with $g \in [AAR, DEF, WATER]$, affecting respectively principal stresses of tension and compression.

- Shear and compression scalar damage (D^s) computed as a function of plastic dilatancy induced by non associated plastic flow due the Drucker-Prager yield function exceeding.

- Damage induced by creep (D^{Cr})

- Damage induced by temperature (D^{Th})

- Last damage are in relation with the re-closure functions of tensile localized cracks. As mentioned in equation 2.5, the re-closure criteria are written in terms of effective stresses, yet these stresses exist only in the crack zone where crack edges roughness are in contact,

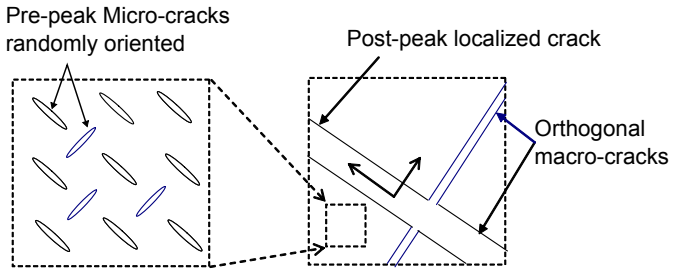

Figure 3.1: Idealized cracking pattern used to compute tensile damages

an anisotropic reclosure damage variable (D^r_{ijkl} in (3.1)) is used to consider only a fraction of compressive stresses are able to cross a localized tensile crack not-yet totally re-closed.

The general form, combining the 10 damages, is given by equation (3.1), where the integrity variables R^i are defined as complementary of damage variables D^i.

$$\sigma_{ij} = \underbrace{\underbrace{\left(1-D^{Cr}\right)}_{R^{Cr}(Creep)}\underbrace{\left(1-D^{Th}\right)}_{R^{Th}(Thermal)}\underbrace{\left(1-D^{s}\right)}_{R^{s}(Shear)}}_{Isotropic\ \ Damages}\left[\underbrace{\underbrace{\left(1-D^{t}_{0}\right)}_{R^{t}_{0}(Pre-peak)}\underbrace{\left(1-D^{t}\right)_{ijkl}}_{R^{t}_{ijkl}(Post-peak)}\prod_{g}\underbrace{\left(1-D^{tg}\right)_{klmn}}_{R^{tg}_{klmn}(g\ /Tension)}\tilde{\sigma}^{+}_{mn}}_{Tensile\ \ Damages}\right.$$
$$\left.+\underbrace{\underbrace{\left(1-D^{r}\right)_{ijkl}}_{R^{r}_{ijkl}(Cracks\ \ Reclosure)}\prod_{g}\underbrace{\left(1-D^{cg}\right)_{klmn}}_{R^{cg}_{klmn}(g\ /Compression)}\tilde{\sigma}^{-}_{mn}}_{Compressive\ \ Damages}\right] \tag{3.1}$$

Due to softening, tensile damage and compressive damage lead to strains localization [32]. The objectivity of FEM solution towards mesh is processed thank to a Hillerborgh method [19]. To avoid dependency of Hillerborgh method toward finite element shape, the model uses an anisotropic description of element size based on the node coordinates [29].

3.1 Damages affecting tensile stresses

As explained above, two types of damage are envisioned:

- a pre-peak isotropic damage can occur if tensile peak strain is greater than the elastic strain at the peak R^t/E
- and in any case, an orthotropic damage occurs during the post peak phase corresponding to the localization of tensile cracks.

The two types of damage are schemed in Figure 3.1.

3.1.1 Pre-peak tensile damage

Isotropic pre-peak damage depends on the principal effective stresses:

$$D^t_0 = 1 - \exp\left(-\frac{1}{m}\left(\frac{\tilde{\sigma}_I}{\tilde{R}^t}\right)^m\right) \tag{3.2}$$

With m a parameter computed such that the behavior law passes by $\sigma_I = R^t$ when $\varepsilon_I = \varepsilon^{peak,t}$. With these conditions the tensile damage value at the peak of stress-strain relation in tension is:

$$D_0^{t,peak} = 1 - \exp\left(-\frac{1}{m}\right) \tag{3.3}$$

This last relation implies the following relationships between parameters and tensile damage at the peak.

$$\begin{cases} \tilde{R}^t = \dfrac{R^t}{1 - D_0^{t,peak}} \\ m = -\dfrac{1}{\ln\left(1 - D_0^{t,peak}\right)} \end{cases} \tag{3.4}$$

D_0^t acts isotropically on the effective stresses tensor, as expressed in (3.1).

3.1.2 Post-peak tensile damages

Localized tensile damages are computed in the principal directions of localized cracks. The orthotropic approximation of localized cracks consists in an idealization of the crack pattern in each element with three orthogonal cracks in three dimensions, (or two orthogonal cracks in two dimensions, as schemed in Figure 3.1). Localized damages depend directly on the maximal crack's openings $w_I^{pl,t,max}$ for $I \in (I, II, III)$.

$$D_I^t = 1 - \left(\frac{w_I^{k,t}}{w_I^{k,t} + w_I^{pl,t,max}}\right)^2 \tag{3.5}$$

with $w_I^{pl,t,max}$ the maximal value of the crack opening $w_I^{pl,t}$, $w_I^{k,t}$ a characteristic crack opening computed such as the dissipated energy during localized damage (rising from 0 to 1) is equal to the fracture energy in tension Gf^t.

$$\begin{aligned} Gf^t &\approx l_I \left(\frac{(R^t)^2}{2E(1 - D_0^t)} + \int_0^\infty (1 - D_0^t)(1 - D_I^t)\tilde{\sigma}_I^+ \mathrm{d}\varepsilon_t^{pl}\right) \\ &\approx l_I \frac{(R^t)^2}{2E(1 - D_0^t)} + R_I^t w_I^{k,t} \end{aligned} \tag{3.6}$$

With R_I^t the tensile strength and l_I the finite element length in the principal direction of cracking I. Different methods can be used to assess l_I. If the model is used with a reinforcement ratio non null (cf. chapter 6.3.2), the fracture energy effectively dissipated in each direction depends on the cracks number in the element (n_I^c given by equation (6.35)). The fracture energy is then anisotropic and given by equation (6.30). Among others, a method based on the Jacobian matrix of geometric transformation from reference to real base was clarified during the Stablon's PhD work and is described in [45]. A simpler method based on the node coordinates of the finite element is given in [29], it consists to project the node coordinates of the finite element in the principal directions I and than to assume $l_I \approx (\max(p) - \min(p))$, with (p) the node coordinate projection on principal direction number I. The value of $w_I^{k,t}$ can be computed for a given finite element with a length l_I using (3.6). This calculus remains possible while the size of the finite element verifies the condition:

$$l_I < \frac{2E(1 - D_0^t)Gf^t}{(R^t)^2} \tag{3.7}$$

If the mesh does not verify condition (3.7), the model adopts a fracture energy Gf_I^{t*} sufficient to avoid a snap back of the behaviour law, so an overestimation of the fracture energy is provoked imposing a softening modulus H at the beginning of localized damage such as:

$$0 > H = \frac{\partial \sigma}{\partial \epsilon} > -\frac{E_0}{n} \tag{3.8}$$

With $n \approx 6$ an arbitrary factor allowing the control of softening branch whatever the finite element size. The consequence of this overestimation is an over-dissipation of fracture energy, but only if the finite element damages. Thanks to this possibility, large finite elements can be used in zones where damage remains small enough to avoid localization. Only the zones where the post peak damage is active have to verify (3.7). It is possible to visualize the zones requiring a finest mesh thanks to an error variable Err_{GF} which is computed and stored in an internal variable Err_{GF}:

$$Err_{GF} = \max_I \left(D_I^t \frac{Gf_I^{t*} - Gf^t}{Gf^t} \right) \tag{3.9}$$

This variable could be used in an automatic meash refinement method for instance.
Damage D_I^t acts on Young modulus, but affects also the Poisson's coefficients as follows [36]:

$$\begin{cases} \varepsilon_{II}^E = \dfrac{C_{IIII}}{1 - D_I^t}\sigma_{II}^+ + C_{IIJJ}\sigma_{JJ}^+ + C_{IIKK}\sigma_{KK}^+ \\ \varepsilon_{IJ}^E = \dfrac{C_{IJIJ}}{1 - \max(D_I^t, D_J^t)}\sigma_{IJ}^+ \end{cases} \equiv \left\{ \varepsilon_{IJ}^E = C_{IJKL}^D \sigma_{KL}^+ \right. \tag{3.10}$$

Relationships (3.10) are defined in the principal directions (I, J, K) of tension plastic strains. On another hand the principle of equivalence in strains proposed in [27] allows to express the effective stresses as a function of elastic strains:

$$\varepsilon_{IJ}^E = C_{IJKL}\tilde{\sigma}_{KL} \tag{3.11}$$

Relations (3.11) and (3.10) allow to compute the integrity tensor components R_{IJKL}^t used in (3.1).

$$(1 - D^t)_{IJKL} = (C^D)^{-1}_{IJMN} C_{MNKL} \tag{3.12}$$

Thank to relation (3.10), the Poisson ratio reductions and Young modules reductions are combined to simulate large crack opening without lateral contraction.

3.1.3 Tensile crack opening

The widths (w_I^{pl}) of localized tensile cracks are computed assuming the tensile plastic strains correspond, in fact, to the permanent crack's openings. In case of radial loading (without change of principal direction), the relationship between a main plastic strain $\varepsilon_I^{pl,t}$ and the corresponding crack's opening is obvious.

$$w_I^{pl} \approx l_I \varepsilon_I^{pl,t} \tag{3.13}$$

This approximation is valid as soon as $\varepsilon_I^{pl,t} \gg$ other strains. Relation (3.13) is no-more usable in case of non-radial loading if the finite element in which the crack appears is not isotropic in terms of size ($l_I \neq l_{II}$), because the rotation of the principal directions need using different

finite element sizes. In this case, it is proposed to compute a crack opening matrix containing the symmetric part of the crack-opening's increments.

$$\frac{\partial \bar{\bar{w}}^{pl}}{\partial t} = \frac{\partial w_I^{pl}}{\partial t}(\overrightarrow{e_I} \otimes \overrightarrow{e_I}) \tag{3.14}$$

Each crack opening increment being computed from the eigenvalues of increment of plastic strain tensor.

$$\frac{\partial w_I^{pl}}{\partial t} = l_I \left(\frac{\partial \varepsilon^{pl,t}}{\partial t}\right)_I \tag{3.15}$$

The maximal crack opening used in Equation (3.5) corresponds to the maximal values of $\overline{\overline{w}}^{pl}$. The actualization process adopted, to compute these maximums, consists in an incremental updating of the normal displacements in the base $(\overrightarrow{e}_1\, \overrightarrow{e}_2\, \overrightarrow{e}_3)$ corresponding to the main directions of $\overline{\overline{w}}^{pl}$.

$$w_{ii}^{pl,max}|_{t+\Delta t} = \max\left(w_I^{pl}|_{t+\Delta t}, w_{ii}^{pl,max}|_t\right) \text{ with } ii \in (11, 22, 33) \tag{3.16}$$

3.1.4 Tensile damages due to over-pressures in the porosity

Internal Swelling reaction and capillary pressure damages are consequences of plastic strains induces by porous over-pressures ($\varepsilon_{ij}^{pl,g} \quad g \in [AAR, DEF, Water]$). The relationship between plastic strains and tensile damages is defined in principal direction of $\bar{\bar{\varepsilon}}^{pl,g}$.

$$D_I^{t,g} = \frac{\varepsilon_I^{pl,g}}{\varepsilon_I^{pl,g} + \varepsilon^{k,g}} \tag{3.17}$$

According to [9], the characteristic strain $\varepsilon^{k,g} \approx 0.3\%$ for AAR and is quasi independent of material. These tensile damages are computed in the principal direction of $\bar{\bar{\varepsilon}}^{pl,g}$.

3.2 Damages affecting compressive stresses

3.2.1 Re-closure damages

Re-closure damages allow to consider the decrease of contacts number between tensile crack edges, so they depend on the crack opening through the principal tensile plastic strains $\varepsilon_I^{pl,t}$.

$$D_I^r = \frac{w_I^{pl,t}\left(w_I^{pl,t} + 2w_I^{k,r}\right)}{\left(w_I^{pl,t} + w_I^{k,r}\right)^2} \tag{3.18}$$

With $w_I^{k,r}$ a characteristic crack opening computed to verify that the energy Gf^r is consumed during re-closing process.

$$Gf^r = l_I \int_{w^{pl,t}}^{0} (1 - D_I^r)\tilde{\sigma}_I^- \mathrm{d}w_I^{pl,t} \tag{3.19}$$

The parameter supplied by the user is the re-closing energy Gf^r. But, this energy can be re-evaluated by the software to insure a stiffness continuity at the end of re-closure:

$$Gf^r \geqslant Gf^{r,min} \text{ with } Gf^{r,min} / \; l_I \left(\frac{\partial\left(\tilde{\sigma}_I^-(1 - D_I^r)\right)}{\partial w_I^{pl,t}}\right)_{w_I^{pl,t}=0} \geqslant E \tag{3.20}$$

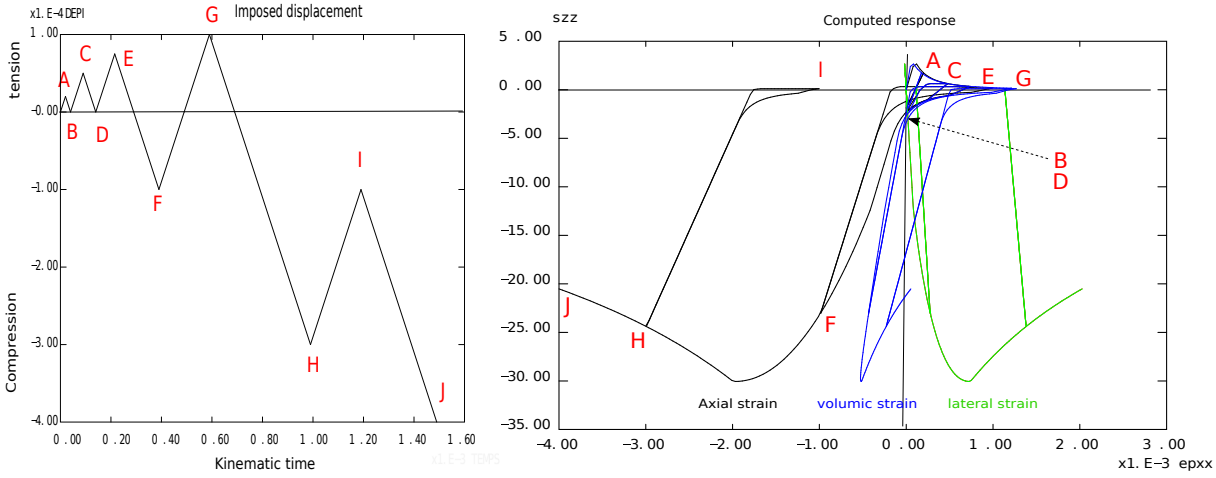

Figure 3.2: Uniaxial-tension-compression cycles with damage, ($R_t = 3MPa$, $R^f = 5MPa$, $R_c = 30MPa$, $\delta = 1$, $\beta = 0.15$, $Gf^t = 100J/m^2$, $Gf^r = 100J/m^2$, $\varepsilon^{k,dc} = 1.e^{-3}$), left figure gives the imposed axial strain versus time, right figure shows the model response: axial stress versus axial strain in black, versus radial strain in green, and versus volume change in blue

Re-closure damage tensor is diagonal in the principal direction of $\bar{\bar{\varepsilon}}^{pl,t}$.

An example of the behaviour law obtained combining the plastic and the damage model is given in Figure 3.2.

3.2.2 Compressive damages due to over-pressures in the porosity

Due to the possibility for cracks to re-close during compressive stresses application, the material is less sensitive to damage in compression than it is in tension. More, it is assumed only cracks perpendicular to the applied direction of compressive stresses play a role, so the damage to apply in compression is deduced from damage in tension as follows:

$$D_I^{c,g} = 1 - \left(\left(1 - D_{II}^{t,g}\right)\left(1 - D_{III}^{t,g}\right)\right)^{\alpha^g} \tag{3.21}$$

g compressive damages in the two other principal directions are obtained by cyclic permutation of subscript (I, II, III). For AAR $\alpha^g \approx 0.15$ is a coupling coefficient quasi independent of material.g compressive damage is a diagonal matrix in the principal direction of $\bar{\bar{\varepsilon}}^{pl,g}$.

3.3 Isotropic damages

3.3.1 Shear damage

Shear damage associated to Drucker Prager criterion is assumed driven by plastic dilatancy $\mathrm{Tr}(\bar{\bar{\varepsilon}}^{pl,s})$. This dilatancy leads to an isotropic damage only if it is greater then a dilatancy threshold ($\varepsilon^{th,s} = \mathrm{Tr}\bar{\bar{\varepsilon}}^{pl,s}_{peak}$) corresponding to the peak in uni-axial compression test:

$$D^s = \begin{cases} \frac{\mathrm{Tr}(\bar{\bar{\varepsilon}}^{pl,s}) - \varepsilon^{th,s}}{\mathrm{Tr}(\bar{\bar{\varepsilon}}^{pl,s}) - \varepsilon^{th,s} + \varepsilon^{k,s}} & if\ \bar{\bar{\varepsilon}}^{pl,s}) > \varepsilon^{th,s} \\ 0 & if\ \bar{\bar{\varepsilon}}^{pl,s}) \leqslant \varepsilon^{th,s} \end{cases} \tag{3.22}$$

With $\varepsilon^{k,s}$ a characteristic strain to control the damage evolution rate versus dilatancy.

3.3.2 Thermal Damage

Thermal activation function C_p^T (1.10) of creep potential amplifies creep for temperature above T_{thr}. The underlying phenomenon is attributed to the contrast of dilation coefficients between different phases which leads to release creep sites in temperature. It is possible this phenomenon comes along with thermal damage, specially if creep site release is due to micro-cracking. So thermal damage D^{Th} and C_p^T are assumed to be linked as follows [24]:

$$D^{Th} = 1 - \frac{1}{A^{Th}\left(C_p^T - 1\right) + 1} \tag{3.23}$$

A^{Th} is a fitting constant to control the damage level at given temperature. In the model, A^{Th} is computed automatically from the measured thermal damage at 80°C in saturated condition (for example in [25], the thermal damage $D^{Th}(80°\text{C}) \approx 0.1$) and A^{Th} can be deduced as follows [11]:

$$A^{Th} = \frac{1}{C_p^T(80°\text{C}) - 1}\left(\frac{S_r D^{Th}(80°\text{C})}{1 - S_r D^{Th}(80°\text{C})}\right) \tag{3.24}$$

S_r is the saturation rate which limits the damage due to temperature if the material is dry.

3.3.3 Creep Damage

Creep damage D^{Cr} allows to consider a coupling between creep strain and possible consequences in terms of macroscopic properties such as apparent stiffness or strength. As the final creep damage D_U^{Cr} is assumed to be linked to coefficient C^M defined in (1.11). The current creep damage depends both on the consolidation variable C_I^C which reflect the current creep strain state and the final creep damage D_U^{Cr}:

$$D^{Cr} = D_U^{cr}\left(1 - \frac{1}{\max(C_I^C, C_{II}^C, C_{III}^C)}\right) \tag{3.25}$$

With C_I^C a consolidation coefficient defined in (1.4).

$$D_U^{Cr} = D_{max}^{Cr}\left(\frac{\tau^{DP}}{\tau_{lim}^{DP}}\right) \tag{3.26}$$

Where D_{Max}^{Cr} is the maximal possible creep damage, linked to the compression strength under long term loading (R_c^{LT}).

$$R_c^{LT} = (1 - D_{max}^{Cr}) \cdot R_c \tag{3.27}$$

In (3.26) τ^{DP} is the equivalent Drucker Prager stress computed with total stress, and τ_{lim}^{DP} the limit Drucker Prager stress deduced from the compression strength like in (2.7).

3.4 Damage visualisation

In order to have a few scalar variables able to summarize the global damage state in tension or in compression, two scalar indicators are build. They are not used in the model, but they give to the user a global view of the material state. The first one summarises the main causes of tensile damages :

$$D^t = 1 - \left(1 - D_0^t\right)\left(1 - D^{Th}\right)\left(1 - D^{Cr}\right)\left(1 - \max\left(D_I^t, D_{II}^t, D_{III}^t\right)\right) \prod_g \left(1 - \max\left(D_I^{t,g}, D_{II}^{t,g}, D_{III}^{t,g}\right)\right) \tag{3.28}$$

The second one combines the different levels of compressive damage :

$$D^c = 1 - (1 - D^s)\left(1 - D^{Th}\right)\left(1 - D^{Cr}\right)\prod_g (1 - \max(\, D_I^{c,g}, D_{II}^{c,g}, D_{III}^{c,g}\,)) \tag{3.29}$$

Chapter 4

Chemistry and Mechanics Coupling

4.1 Hydration

The hydration degree ζ, represents the fraction of material able to support a stress. It ranges from zero for not solidified matrix until one for a complete solidification. Several material parameters are linked to the hydration thanks to the De Schutter evolution law [15] :

$$\frac{X}{X^{ref}} = \left(\frac{\zeta - \zeta^{th}}{\zeta^{ref} - \zeta^{th}} \right)^{n^X} \tag{4.1}$$

With ζ^{th} the solidification threshold, $\zeta^{ref} = 1$ the reference hydration degree for which are given the material parameters, n^X a non linearity exponent for material parameter X. X^{ref} the value of X for ζ^{ref}. The hydration acts also on internal variable as explained in [7]. In

Parameter X	Symbol	Exponent n^X
Young modulus	E	0.66
Poisson coefficient	$0.45 - \nu$	0.66
Tensile strength	Rt	0.66
Re-closure characteristic stress	σ^r	0.66
Compressive strength	Rc	0.66
Confinement coefficient for DP criterion	δ	0.00
Dilatancy coefficient for non associated plasticity	β	0.00
(1-Biot)	$1 - b$	0.50
Van Genuchten modulus	M_{shr}	1.86
Fracture energy	Gf_t	0.50
Crack reclosure energy	Gf_r	0.50

Table 4.1: Exponents of De-Schutter law for material parameters

fact, as internal variables of the model concern both the hydrated and un-hydrated parts, each of them is considered as the average value between hydrated and un-hydrated parts of the elementary volume of material, this leads to the following updating conditions:

$$\frac{\partial V_i}{\partial \zeta} = -\frac{V_i}{\zeta} \tag{4.2}$$

In(4.2) V_i is an internal variable of the model. This updating condition is applicable to almost all the internal variables, except the chemical ones. The list of internal variables updated in case of evolution of the hydration degree are given in subroutine *'hydravar3d'*.

4.2 Water content

The tensile strength depends on the water content through a linear law :

$$Rt = Rt^{sat} - k^{w,Rt} b^w p^w \tag{4.3}$$

According to MOSAIC ANR research program [6], $k^{w,Rt} \approx 0.25$ for concrete. Note, the formulation takes into account the decrease of positive effect of capillary pressure on Rt with the temperature rising, because, as explained by equation (1.18), the capillary pressure decreases with the temperature rise [11].

4.3 Internal Swelling Reactions

4.3.1 Chemical advancement of Internal Swelling Reaction

Chemical advancement of the alkali aggregate reaction

The chemical advancement of AAR depends on temperature and humidity. The internal variable A^{aar} gives the chemical advancement rate, starting from 0 for sound material until 1 when the alkali aggregates reactions are ended.

$$\frac{\partial A^{aar}}{\partial t} = \frac{1}{\tau^{aar}_{ref}} C^{T,aar} C^{W,aar} \left(A^{aar,\infty} - A^{aar}\right) \tag{4.4}$$

- $C^{T,aar}$ the thermal activation coefficient modeled thank to the Arrhenius law:

$$C^{T,aar} = \exp\left(-\frac{E^{aar}}{R}\left(\frac{1}{T} - \frac{1}{T_{ref}}\right)\right) \tag{4.5}$$

  With $E^{aar} \approx 40000 J/Mol$ the activation energy of chemical processes involved in the reaction, T^{ref} the absolute reference temperature for which the characteristic time τ^{aar}_{ref} is fitted.

- $C^{W,aar}$ takes into account the reduction of kinetic when material is not water saturated:

$$C^{W,aar} = \begin{cases} \left(\dfrac{S_r - S_r^{th,aar}}{1 - S_r^{th,aar}}\right) & \text{if } S_r > S_r^{th,aar} \\ 0 & \text{if } S_r \leqslant S_r^{th,aar} \end{cases} \tag{4.6}$$

  S_r the water saturation rate, $S_r^{th,aar}$ the saturation rate threshold under which the reaction kinetic is null.

- $A^{aar,\infty}$ is the maximal advancement of the reaction, based on experimental works of Poyet et al [33] it assumes only the reactive site in contact with liquid water can react:

$$A^{aar,\infty} = S_r \tag{4.7}$$

The amount of gel involved in the swelling processes depends both on the chemical advancement of the reaction A^{aar} and on the gel production potential of material:

$$\phi^{aar} = \phi^{aar,\infty}.A^{aar} \tag{4.8}$$

With $\phi^{aar,\infty}$ the gel production potential which is a characteristic of material.

Chemical advancement of Delayed Ettringite

The delayed ettringite is the consequence of a hot period during which the primary sulfo-aluminate hydrates are dissolved, releasing sulphates and aluminates in the pore solution. These ions are then adsorbed or combined more or less definitively in the other hydrates. If the hot period is long enough, according to [35] a part of the aluminate ions could combine with C-S-H to form hydro-garnet or with lime aggregate to form Carbo-Alumintes. As hydro-garnets and Carbo-Aluminates are stable in temperature [16], their combined aluminates are no more available for delayed ettringite. If the hot period is not long enough or the temperature too low, there is not enough time to convert aluminates in these stable forms, so they can recombine with sulphates when the temperature comebacks to a low level. This phenomenon explains the existence of a pessimum in terms of hot period duration. If the hot period is short only a few primary sulfo-aluminates are dissolved, if the hot period is very long, all the primary sulfo aluminates are dissolved, but aluminates can be combined in stable forms, so only intermediate hot period durations can lead to a maximum of delayed ettringite. Therefore, according to [43] the numerical implementation of an ettringite model can be based on two equations sets:

- A first one dedicated to the calculation of dissolution of primary sulfo-aluminates and to the assessment of aluminates bonding in stable froms.
- A second one aiming to model the precipitation of delayed sulfo-aluminates.

Dissolution of sulfoaluminates As shown by Kchakech, Martin et al. in [22], the temperature above the sulfo-aluminates dissolves depends on the alkali concentration in the pore solution as follows :

$$T^{th,def}[K] = \begin{cases} T^{k,def}\left(\dfrac{Na^k}{Na}\right)^{-n} & \text{if } Na \geqslant Na^k \\ T^{k,def} & \text{if } Na < Na^k \end{cases} \tag{4.9}$$

With $Na^k \approx 0.28 mol/l$, $n \approx 0.18$ and $T^{k,def} \approx 80°\text{C}$. The dissolution rates of primary ettringite and monosulfoaluminates (E^1 and M^1 respectively) are assumed to be close and equal to thus of delayed ettringite (E^2), so that a single characteristic time can be used for all of them in a first order kinetic equation:

$$\begin{cases} \dfrac{\partial E^1}{\partial t} = -\dfrac{E^1}{\tau^{Diss}} \\ \dfrac{\partial M^1}{\partial t} = -\dfrac{M^1}{\tau^{Diss}} \\ \dfrac{\partial E^2}{\partial t} = -\dfrac{E^2}{\tau^{Diss}} \end{cases} \tag{4.10}$$

In (4.10), τ^{Diss} is the characteristic time for the dissolution velocity; it depends on temperature (T) and alkali content (Na):

$$\tau^{Diss} = \frac{\tau^{Diss,ref}}{C^{T,Diss} C^{Na,Diss}} \tag{4.11}$$

$\tau^{Diss,ref}$ is a kinetic constant characterizing the material transfer properties at the micro-scale where the dissolution processes take place, in [43] a value close to $3days$ is fitted on experimental results from [22] and [5] ; $C^{T,Diss}$ considers the effect of temperature on the dissolution velocity as follows :

$$C^{T,Diss} = \exp\left(-\frac{E^{a,Diss}}{R}.\left(\frac{1}{T} - \frac{1}{T^{th,def}}\right)\right) - 1 \ \geq 0 \tag{4.12}$$

With $E^{a,Diss}$ the activation energy for the dissolution processes (close to $70000J/mol$ according to [43]), R the gaz constant, T the absolute temperature and $T^{th,def}$ the threshold temperature given by (4.9). In (4.10) $C^{Na,Diss}$ considers the positive effect of alkali on the dissolution kinetic through the following expression :

$$C^{Na,Diss} = \left(\frac{Na}{Na^k}\right) \tag{4.13}$$

The aluminates released by the dissolution of sulfo-aluminates phases are noted $\tilde{A}$. As they are partially re-absorbed to form hydro-garnets stable in temperature, only a part of them are available to form delayed ettringite at long term during the cold periods. The amount of remaining aluminates is assessed as follows:

$$\frac{\partial \tilde{A}}{\partial t} + \frac{\tilde{A}}{\tau^{Fix}} = -\left(\frac{\partial E^1}{\partial t} + \frac{\partial M^1}{\partial t} + \frac{\partial E^2}{\partial t}\right) \tag{4.14}$$

With τ^{Fix} the characteristic time for the fixation of aluminates in hydro-garnets. This parameter depends on temperature according to coefficient $C^{T,Fix}$, and on alkali content through $C^{Na,Fix}$ as follows:

$$\tau^{Fix} = \frac{\tau^{Fix,ref}}{C^{T,Fix} C^{Na,Fix}} \tag{4.15}$$

With $\tau^{Fix,ref}$ a material constant. In [43] a value close to $3days$ is proposed, and $C^{Na,Fix}$ given by :

$$C^{Na,Fix} = \left(\frac{Na^k}{Na}\right)^m \tag{4.16}$$

$m \approx 3$ a fitting parameter. $C^{T,Fix}$ considers the effect of temperature:

$$C^{T,Diss} = \exp\left(-\frac{E^{a,Fix}}{R}.\left(\frac{1}{T} - \frac{1}{T^{th,Fix}}\right)\right) - 1 \ \geq 0 \tag{4.17}$$

In (4.17) $E^{a,Fix} \approx 180000J/mol$ is the activation enerfy, and $T^{th,Fix} \approx 70$C the threshold temperature for the aluminate fixation.

The amount of sulphates released by the dissolution processes are noted $\tilde{S}$, and directly deduced from (4.10) as follows:

$$\frac{\partial \tilde{S}}{\partial t} = -3\left(\frac{\partial E^1}{\partial t} + \frac{\partial E^2}{\partial t}\right) - \left(\frac{\partial M^1}{\partial t}\right) \tag{4.18}$$

Precipitation of sulfoaluminates If the condition required are satisfied ($T < T^{th,def}$ see. (4.9)), the delayed ettringite can precipitate. The precipitation kinetic is assumed controlled by the sulfate supply:

$$\frac{\partial E^2}{\partial t} = \frac{\tilde{S}}{\tau^{Prec}} \mathcal{H}\left(\max\left(M^1, \tilde{A}\right)\right) \tag{4.19}$$

$\mathcal{H}\left(\max\left(M^1, \tilde{A}\right)\right)$ is the Heaviside function which takes into account the presence of aluminium available for the DEF. The model gives the priority to the conversion of M^1 into secondary ettringite until M^1 is totally depleted. Next the consumption of $\tilde{A}$ starts until the total depletion of $\tilde{A}$ or $\tilde{S}$:

- While $M^1 > 0$ and if $\tilde{S} > 0$:

$$\begin{cases} \dfrac{\partial M^1}{\partial t} = -\dfrac{\partial E^2}{\partial t} \\ \dfrac{\partial \tilde{S}}{\partial t} = -2\dfrac{\partial E^2}{\partial t} \\ \dfrac{\partial \tilde{A}}{\partial t} = 0 \end{cases} \tag{4.20}$$

- When $M^1 = 0$ and while $\tilde{A} > 0$ and $\tilde{S} > 0$:

$$\begin{cases} \dfrac{\partial M^1}{\partial t} = 0 \\ \dfrac{\partial \tilde{S}}{\partial t} = -3\dfrac{\partial E^2}{\partial t} \\ \dfrac{\partial \tilde{A}}{\partial t} = -\dfrac{\partial E^2}{\partial t} \end{cases} \tag{4.21}$$

In (4.19), τ^{Prec} is the characteristic time of the reactions. It depends on the temperature, the alkali content and the water content as follows:

$$\tau^{Prec} = \frac{\tau^{Prec,ref}}{C^{T,Prec}.C^{Na,Prec}.C^{W,Prec}} \tag{4.22}$$

$\tau^{Prec,ref}$ is a material constant (a characteristic time of the reaction), $C^{T,Prec}$ considers the effect of the temperature on the precipitation rate as follows:

$$C^{T,Prec} = \frac{C^{T,Diss}\left(T\right)}{C^{T,Diss}\left(T^{ref,Prec}\right)} \exp\left(-\frac{Ea^{prec}}{R}\left(\frac{1}{T} - \frac{1}{T^{ref,Prec}}\right)\right) \tag{4.23}$$

Ea^{prec} is the activation energy for the precipitation process, and $T^{ref,Prec}$ the reference temperature for the characteristic time of precipitation. $C^{Na,Prec}$ considers the limiting effect of alkali which, at high concentration is able to prevent the DEF. In fact in presence of Portlandite, the alkali control the amount of Calcium in solution and privilege the adsorption of sulphate in the cement matrix versus its availability for DEF:

$$C^{Na,def} = \begin{cases} \left(1 - \dfrac{Na)}{Na^{th,def}}\right)^m & \text{if } Na < Na^{th,def} \\ 0 & \text{if } Na \geqslant Na^{th,def} \end{cases} \tag{4.24}$$

In equation (4.24), $Na^{th,def} \approx 0.92mol/l$ is a threshold value beyond which the DEF formation is stopped. The exponent $m \approx 3$" considers the non linearity of this phenomenon. $C^{W,Prec}$ is computed according to the following equation which consider the better diffusion of ions in saturated porosity:

$$C^{W,Prec} = \exp\left(-\frac{1-Sr}{1-Sr^k}\right) \tag{4.25}$$

With Sr^k a material parameter which controls the decrease of precipitation rate according to the saturation rate Sr. Experimental program cariied out by AlShama et al. in [1] [2] shows that DEF needs a very high humidity level corresponding to $(0.9 < Sr^k < 0.99)$. The volume of delayed products considered in the poromechanical model is deduced from the moles number of each type:

$$\frac{\partial \phi^{def}}{\partial t} = \frac{\partial E^2}{\partial t} V_{AFt} + \frac{\partial M^1}{\partial t} V_{AFm} \tag{4.26}$$

With $V_{AFt} \approx 715cm^3/mol$ and $V_{AFm} \approx 254cm^3/mol$ the molar volume of ettringite and monosulfoaluminate, respectively.

Initial conditions On one hand, the amount of aluminium and sulphates are not always known for an existing structure affected by the DEF, and on the other hand the damage state or the swelling of the structure can be known. So to facilitate the chemical data assessment, the form chosen to supply them consists to specify the Sulphate versus aluminium mole number ratio ρ and the maximal DEF volume creatable $\phi^{Def,Max}$ in optimal conditions.

$$\rho = \frac{SO_3}{Al_2O_3} \tag{4.27}$$

ρ of a cement is generally ranged in $[0.5 - 1]$ Supplying this last parameter allows the user to use the poro-mechanical coupling to feet the DEF potential of the material independently of its hydration degree, and in accordance with the observed mechanical effects, without ignoring the Sulphate/Aluminium ratio which is the main parameter acting on the hot period pessimal duration. To pass from the couple $\rho, \phi^{Def,Max}$ to the couple $S^c = SO_3$, equivalent $A^c = Al_2O_3$. The following assumptions are made:

- If $\rho > 3$ the aluminium mole number limits the DEF amount, and the chemical data are obtained as follows:

$$\begin{cases} A^c = \frac{\phi^{Def,Max}}{VAFt} \\ S^c = \rho A^c \end{cases} \tag{4.28}$$

- If $\rho \leqslant 3$ the sulphate moles number limits the production of DEF:

$$\begin{cases} S^c = 3\frac{\phi^{Def,Max}}{VAFt} \\ A^c = \frac{S^c}{\rho} \end{cases} \tag{4.29}$$

Once these amount assessed, the moles number of primary hydrates are deduced as follows, and used as initial conditions for the dissolutions equations (4.10) (4.14) (4.18).

- If $S^C > 3A^c$, the initial hydration products contain sulfoaluminates mainly in ettringite form:

$$\begin{cases} E^1 = A^c \\ M^1 = 0 \\ \tilde{S} = S^c - 3E1 \\ \tilde{A} = 0 \end{cases} \tag{4.30}$$

- $S^C < A^c$, the initial hydration products contain sulfoaluminates mainly in monosulfoaluminate form:

$$\begin{cases} E^1 = 0 \\ M^1 = S^c \\ \tilde{S} = 0 \\ \tilde{A} = A^c - M^1 \end{cases} \tag{4.31}$$

- In the other intermediates cases, primary ettringite and monosulfoaluminates coexist:

$$\begin{cases} E^1 = \frac{S^c - A^c}{2} \\ M^1 = \frac{3A^c - S^c}{2} \\ \tilde{S} = 0 \\ \tilde{A} = 0 \end{cases} \tag{4.32}$$

The other internal variable (E^2) is set to zero as initial condition, its evolution is controlled by (4.19) which acts also on $\tilde{S}$ and $\tilde{A}$ through equations (4.21). Users have also the possibility to impose the mole number of sulphates $S^c = S^c_{imp}$, in this case the number of aluminates is computed directly according to ρ:

$$Ac = \frac{S^c_{imp}}{\rho} \tag{4.33}$$

If the imposed mole number of sulphates is not in accordance with the mole number of sulphates deduced from (4.29) then a compatibilty coefficent is automatically computed and affected to the volume of delayed ettringite:

$$C^D_{eff} = \frac{S^c}{S^c_{imp}} \tag{4.34}$$

As the imposed mole number of sulphates is assumed prevalent compared to the mole number deduced from (4.29), the coefficent C^D_{eff} should allways be greater than 1, so if $C^D_{eff} < 1$ a warning message is printed and the program stops.

Environmental conditions Temperature T, alkali content Na and saturation rate Sr must be supplied as data to the chemical evolution model. They can be computed before the chemo-mechanical or together, depending on the coupling level chosen by the user.

4.3.2 Pressure induced by Internal Swelling Reactions

The alkali reaction or the delayed ettringite lead to the production of new phases ϕ^g. As the connected porosity volume is affected by the global volume change induced by the deformation,

the gel pressure depends on the strain state :

$$p^g = M^g \left(\phi^g - \left(\phi_0^g \frac{p^g}{C^g Rt} + b^g \mathrm{Tr} \left(\varepsilon - \left(\varepsilon^{p,t} + \varepsilon^{p,c} \right) \right) + (1 - b^g) \, \mathrm{Tr}(\varepsilon^{p,g}) \right) \right) \tag{4.35}$$

Equation (4.35) has to verify the condition $p^g \geq 0$, with ϕ_g the phase volume fraction amount assessed from the chemical advancement of the reactions, and computed for AAR gel production by equation (4.8) and for DEF production by equation (4.26):

$$\phi_g = \phi^{aar} \quad or \quad \phi^{def} \tag{4.36}$$

In (4.35), b^g is the Biot coefficient approximation supplied by a homogenization method:

$$b^g \approx \frac{2\phi^g}{1 + \phi^g} \tag{4.37}$$

and M^g the Biot modulus linked to the Biot coefficient and compressibility moduli as follows:

$$\frac{1}{M^g} = \frac{b^g - \phi^g}{K^s} + \frac{\phi^g}{K^g} \tag{4.38}$$

with K^g the compressibility modulus of the new phase and K^s the compressibility of the matrix defined as the material deprived of the volume occupied by the gel:

$$K^s \approx \frac{E}{3(1 - 2\nu)} \frac{1}{1 - b^g} \tag{4.39}$$

with E the Young modulus of the material and ν its Poisson coefficient. In (4.35), ϕ_0^g is the available porosity connected to the reactive site where the new phase g is created. This volume of connected porosity is filled under a pressure $p^g = C^g Rt$, with C^g the stress concentration factor defined in (2.6). If the pressure p^g exceeds $C^g Rt$ the filled volume increases above ϕ_0^g; In tri-axial confinement, the plastic criteria (2.6) cannot be activated and the plastic flow modelled by $\varepsilon^{p,g}$ does not occur, limiting the swelling to its elastic part, else the plastic criteria (2.6) can be activated and the plastic flow of $\varepsilon^{p,g}$ occurs, leading to a larger swellings due to micro-cracking. As the micro-cracks are assumed connected to the reactive site, their volume can be reached by the reactive product, modifying the pressure according to (4.35).

Chapter 5

Probabilistic scale effect in tension

5.1 Principle

The spatial random distribution, corresponding to material heterogeneity, leads to a probabilistic scale effect as soon as the behaviour law present a softening phase. This scale effect can be treated simply using a random field of tensile strength (direct random sampling or mesoscopic modelling of random distribution of heterogeneities). But as random sampling based methods need a large enough sample to have a reliable representation of the model behaviour, they are time consuming. So, an alternative method, called "Weakest Link Localization" is proposed bellow.

5.2 Weibull scale effect

This method avoids resorting to a mesoscopic modelling or to a random fields sample. The Weakest Link localization method (WL2 [42]) allows to assess directly the most likely tensile strength using the Weibull's concepts. In the Weibull theory the tensile strength to be used depends on the loaded volume (V^{eq}) through the scale effect law:

$$\frac{Rt}{Rt^{ref}} = \left(\frac{V^{eq}}{V^{ref}}\right)^{-\frac{1}{m}} \tag{5.1}$$

In this scale effect law Rt^{ref} is the average tensile strength measured with a specimen for which the loaded volume is V^{ref}. m is the Weibull exponent which depends on the coefficient of variation (C^v) of experimental results:

$$C^v = \frac{\sqrt{\Gamma\left(1+\frac{2}{m}\right) - \Gamma^2\left(1+\frac{1}{m}\right)}}{\Gamma\left(1+\frac{1}{m}\right)} \tag{5.2}$$

This relation admits the following inverse approximation, more useful to compute the Weibull exponent (m) as a function of the coefficient of variation (Cv) of experimental results :

$$m \approx \frac{1}{10}\left(\frac{12}{C^v} - 2\right) \tag{5.3}$$

5.3 Weakest Link Localization method (WL2)

5.3.1 Principle

The WL2 method consists to assess the equivalent loaded volume V^{eq} using a modified Weibull theory. The modification proposed in [42] consists to use a weighting function which considers a non-homogeneous probabilistic influence of material points (M) towards each other (located at a distance $d(M)$) in equation (5.4). The weighting function ψ (5.4), accords a larger probabilistic importance to the vicinity of any material point.

$$\psi(M) = \exp\left(-\frac{1}{2}\left(\frac{d(M)}{l^{cp}}\right)^2\right) \tag{5.4}$$

With $d(M)$ the distance between any damageable material point, for instance located at M, and any other point of the structure located at the distance $d(M)$ from M. l^{cp} is the characteristic length of the probabilistic weighting function; it is assessed from $0.3 \rightarrow 0.5$ meters for a concrete in [42]. The equivalent loaded volume is then defined as follows:

$$V^{eq}(M) = \frac{1}{\beta^{max}} \underbrace{\int_{\Omega} \beta\psi(M)d\Omega}_{\overline{\alpha}} \tag{5.5}$$

With Ω the structure, $d\Omega$ a structure infinitesimal volume. β is the loading index defined at each integration point as follows:

$$\beta = \left(\frac{\max(\sigma_I, 0)}{Rt^{ref}}\right)^m \tag{5.6}$$

In (5.6), if the loaded index β is evaluated in a zone already damaged, it is limited to the unit to consider that as in this zone the tensile strength is known, the probabilistic weight of the residual undamaged zone around the integration point must be limited. With σ_I the principal tensile stress. If the structure volume (Ω) is very large compared to the characteristic length l^{cp}, and the stress field homogeneous, the equivalent loaded volume tends to a maximal equivalent loaded volume V^{max} impossible to exceed whatever the stress field in the structure and the real size of the structure:

$$V^{max}(M) = \int_{\Omega} \psi(M)d\Omega \tag{5.7}$$

Due to the geometry boundary effects,$V^{max}(M)$ is smaller near the geometry faces and edges. Consequently $V^{max}(M)$ is a non homogeneous scalar field. It can be assessed with an integral operator before the non-linear analysis. In CASTEM, the integral operator 'NLOC' allows to compute the $V^{max}(M)$ field before the non linear analysis. Note, the operator 'CONN' is able to consider symmetry plans and symmetry axis of the finite element model to establish a connectivity map exploited by the operator 'NLOC' to compute the $V^{max}(M)$ field.

5.3.2 Implementation with an Helmholtz formulation

In [42], it is proposed to assess the equivalent loaded volume V^{eq} thanks to a second gradient formulation:

$$\overline{\alpha} - \frac{l^{cp^2}}{2} \bigtriangledown \overline{\alpha} = \beta V^{max} \tag{5.8}$$

Once the non local loading variable $\overline{\alpha}$ computed, the equivalent loaded volume is deduced:

$$V^{eq}(M) = \frac{\overline{\alpha}}{\beta^{max}} \tag{5.9}$$

In equation (5.9), β^{max} is the maximal loading index over the structure.

5.4 Numerical Implementation of the Weakest Link Localization method

5.4.1 Semi-implicit procedure

Once $V^{eq}(M)$ computed, it is used in the Weibull scale effect law (5.1) to assess the most likely tensile strength field. The operation has to be performed during each loading increment to adapt the tensile strength to the current loading. As the most likely tensile strength depends on the stress field in the undamaged zone, but as these zones are susceptible to damage during the non-linear analysis, a first approximation of the stress field is performed using the tensile strength field of the previous time step, then a non local sub-step is performed using this field to assess a more accurate tensile strength field. The definitive calculus is done with this last one. This formulation is available in CASTEM software using the Non-Local formulation with the keyword $HELM$. If this formulation is not used the WL2 method is not activate and the model works without considering the probabilistic scale effect.

5.4.2 Use of the Helmholtz equation in case of evolutive matrix

In equation (5.5) and (5.6),the denominator Rt^{ref} can be simplified, showing that the equivalent loaded volume depends only on the stress field form, and not of its amplitude. On the other hand, when the matrix damages, abd as the scale effect affects only the matrix zone not yet damaged, a special treatment is done to consider that in a given finite element the Weibull scale effect could evolves during the damage process. On purpose an updating method is used during the time step Δt:

$$\left(\frac{Rt}{Rt^{ref}}\right)_{t_0+\Delta t} D^t_{t_0+\Delta t} = \left(\frac{Rt}{Rt^{ref}}\right)_{t_0} D^t_{t_0} + \left(\frac{Rt}{Rt^{ref}}\right)\left(D^t_{t_0+\Delta t} - D^t_{t_0}\right) \tag{5.10}$$

5.4.3 Limit of scale effect for small equivalent loaded volume

Several methods are implemented to allow a compatibility between criteria. In fact, for small equivalent loaded volume (Veq), the Weibull scale effect (5.1) leads to an increase of the tensile strength, and in another hand the compressive strength is assumed independent of the loaded volume. A consequence could be a modification of the ratio between the tensile and the compressive strength. However this ratio must stay in the limit needed to have an independence between the Drucker Prager and the Rankine criteria. This limit is verified during the plastic criteria assessment. If the tensile strength is locally higher then the limit, it can be limited locally to the value needed to avoid the interaction.

Chapter 6

Distributed reinforcements

6.1 Principle

To avoid or limit explicit meshing of reinforcements, their structural effects can be considered as equivalent to the ones due to orthotropic distributed reinforcements. The distributed reinforcement directions are noted ($\overrightarrow{V^r}$, with $r \in [1..n^r]$). n^r the distributed reinforcements number. In each direction a reinforcement rate ρ^r is considered, it corresponds to the cross section rate of the reinforcements r oriented along the axe ($\overrightarrow{V^r}$).

6.2 Homogenized behaviour law of a reinforced matrix

If the distributed reinforcements are used in the context of damage mechanics, and if localized cracks can occur, then, if a crack's normal and a reinforcements are not aligned, as illustrated in figure 6.1, a dowel effect takes place, changing the reinforcement orientations into the cracks and closely. Elsewhere, the reinforcements stay aligned on their initial directions. Therefore, two cases have to be considered, one corresponding to the reinforcements contribution into the zones without localized cracks, and another-one into the localized cracks. As the two zones can coexist in a finite element, the combination method adopted consists to weight the dowel effect by the localized damage and the contribution into undamaged zone by its complement to the unit. The sum is done using the four order tensor D^t taking into account the localized cracks, as expressed by (6.1).

$$\sigma_{ij} = (1 - \sum_r \rho^r)\sigma^m_{ij} + (1 - D^t_{ijkl})\sigma^H_{kl} + D^t_{ijkl}\sigma^R_{kl} \tag{6.1}$$

In (6.1), σ^H is the homogenized stress induced by the reinforcements in the undamaged zone, given by Eq. (6.2). σ^R if the stress state corresponding to the bridging of localized cracks by the reinforcements, given by Eq. (6.3).

6.2.1 Reinforcements contribution in undamaged zone

The homogenized behaviour law of the reinforced matrix assumes the distributed reinforcements contributions have an axial component σ^r induced by the reinforcement elongation in the direction $\overrightarrow{V^r}$. The contribution of a reinforcement is then directly proportional to its rate

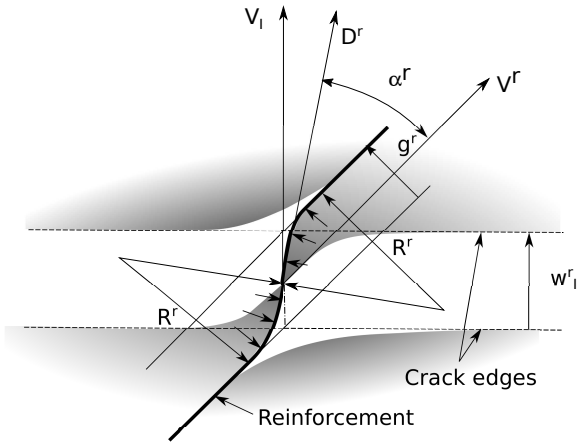

Figure 6.1: Dowel effect

ρ^r. The combination is done using a mix proportion of the normal stress in the matrix (σ_r^m) and in the reinforcements:

$$\sigma_{ij}^H = \sum_r \rho^r \sigma^r \left(\overrightarrow{V^r} \otimes \overrightarrow{V^r}\right)_{ij} \tag{6.2}$$

6.2.2 Reinforcements contribution in localized cracks

In case of damage, the reinforcement orientation can be modified into the crack if the crack's normal is not aligned with the reinforcement. This is the dowel effect illustrated in 6.1, and modelled through a mis-alignment of the reinforcement force into the cracks (relatively to the initial orientation of the reinforcement). The orientation of the reinforcement into the crack I is noted $\overrightarrow{D_I^r}$. The method consists to replace the matrix contribution into the cracks by the reinforcement contributions. Due to the minimal value of curvature radius induced by the interaction between the reinforcement and the matrix, the orientation of the reinforcement into the crack is always comprised between the reinforcement direction into the matrix and the direction normal to the crack. Thanks to the orthotropic model adopted to consider localized cracks effects, the cracks orientations are known and noted $\overrightarrow{V^I}$. In each crack the contributions of all the reinforcements crossing the crack are affected by the corresponding localized damage, summed up, and expressed into the base of localized damage thanks to the passage matrix $\mathbf{P}$. A first non symmetrical matrix $\mathbf{R}$ is obtained (6.3).

$$\begin{aligned}\mathbf{R} = \sum_r \rho^r \sigma^r \mathbf{P}^T \left[D_I^t \left(\overrightarrow{V^r}.\overrightarrow{V^I}\right) \overrightarrow{D_I^r}\right] ; \mathbf{P}^T \left[D_{II}^t \left(\overrightarrow{V^r}.\overrightarrow{V^{II}}\right) \overrightarrow{D_{II}^r}\right] ; \\ \mathbf{P}^T \left[D_{III}^t \left(\overrightarrow{V^r}.\overrightarrow{V^{III}}\right) \overrightarrow{D_{III}^r}\right]\end{aligned} \tag{6.3}$$

The effective contributions of reinforcements into the cracks is then taken equal to the symmetrical part of $\mathbf{R}$ (6.4) .

$$D_{ijkl}^t \sigma_{kl}^R = \left[\mathbf{P}\left[\frac{1}{2}\left[\mathbf{R} + \mathbf{R}^T\right]\right]\mathbf{P}^T\right]_{ij} \tag{6.4}$$

Equation (6.4) is based on the fact that the dowel effect can exist only if a misalignment of a given reinforcement is balanced by a compressive link in the matrix which is itself blocked by

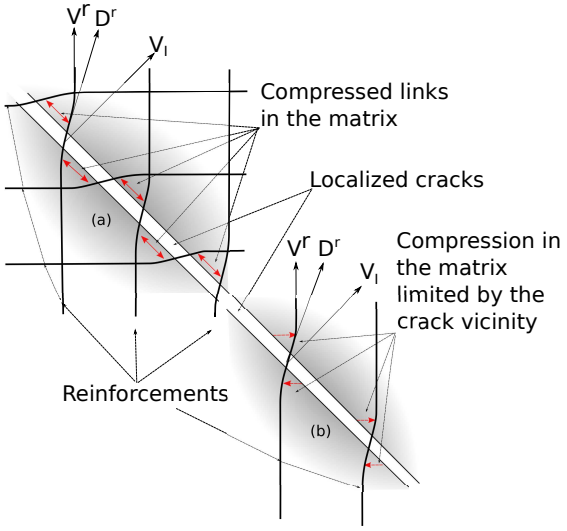

Figure 6.2: Compressed links in the matrix allowing dowel effect (a) or limiting dowel effect (b)

another reinforcement with a different orientation as illustrated in figure 6.2(a). The misalignment of at least one-another reinforcement crossing the same crack or another crack is then needed. If a reinforcement is alone to cross a given crack the compressive link in the matrix needed to change the reinforcement orientation, which is quasi orthogonal to the reinforcement, cannot be balanced, and the reinforcement direction cannot be changed, as illustrated in figure 6.2(b). That is why in Eq.(6.4), only the symmetrical part of the matrix is assumed admissible. If a single reinforcement crosses a single crack with a given relative inclination, the force orientation in the reinforcement is not aligned to the normal to the crack, but, as the equilibrium needed to have a dowel effect is possible only if the compressive links are balanced, the dowel effect must be reduced, what is done by the symmetrization operation (6.4) which in such a case divide by two the shear contribution of the reinforcement into the crack. In (6.3), the direction of the reinforcement into the crack $\overrightarrow{D_I^r}$ is a combination between the geometric (initial) direction of the reinforcement $\overrightarrow{V_r}$ and the normalized value of the lateral displacement $\overrightarrow{g_I^r}$ induced by the dowel effect :

$$\overrightarrow{D^r} = cos(\alpha^r)\overrightarrow{V_r} + sin(\alpha^r)\frac{\overrightarrow{g_I^r}}{||\overrightarrow{g_I^r}||} \tag{6.5}$$

The lateral displacement $\overrightarrow{g_I^r}$ is the difference between the crack opening displacement and its own projection on the initial direction of the reinforcement:

$$\overrightarrow{g_I^r} = w_I^{pl,t}\left(\overrightarrow{V_I} - \left(\overrightarrow{V^r}.\overrightarrow{V_I}\right)\overrightarrow{V^r}\right) \tag{6.6}$$

The angle α^r between the reinforcement reorientation into the crack $\overrightarrow{D^r}$, and its original direction $\overrightarrow{V^r}$, depends on the curvature radius R^r of the reinforcement on both sides of the crack, as illustrated in figure 6.1.

$$\alpha^r = 2\arcsin\left(\sqrt{\frac{g_I^r}{4R^r}}\right) \leqslant \arccos\left(|\overrightarrow{V_I}.\overrightarrow{V^r}|\right) \tag{6.7}$$

R^r is assessed using a based strap relationship, considering the tension in the reinforcement σ^r,the reinforcement diameter D_r^{eq} and the concrete compressive stress fc:

$$R^r = \frac{\pi D_r^{eq} \sigma^r}{4fc} \tag{6.8}$$

Note, the method to assess the misalignment uses only the current crack opening $w_I^{pl,t}$. Another method could consist to project the maximal crack openings $w_I^{pl,t,max}$ in the principal base of the current opening, and add the shear component of the difference between these two tensors expressed in this base to consider the dowel effect even if cracks are re-closed, but as reinforcement's stresses remove also during re-closure processes, and as reinforcement's contribution is proportional to these stresses, the adopted formulation is an a priori admissible approximation.

6.3 Axial stress in a reinforcement

6.3.1 Constitutive equation for the reinforcement material

The behaviour law of reinforcements is elasto-plastic with a linear kinematic hardening and a relaxation law. It is given in each direction of reinforcement by equation (6.9):

$$\sigma^r - \sigma_0^r = E^r(\epsilon^r - \epsilon^{r,pl} - \epsilon^{r,m} - \epsilon^{r,k}) \tag{6.9}$$

With E^r the reinforcement Young modulus, ϵ_i^r the axial strain in the reinforcement, $\epsilon^{pl,r}$ its plastic strain,$\epsilon^{r,m}$ its permanent viscous strain and $\epsilon^{r,k}$ its reversible viscous strain. σ_0^r is the possible pre-stress applied to the reinforcement as initial stress (not induced by the computed strain field).

Reinforcements plasticity

The plastic criterion is uni-axial, it models a linear kinetic hardening (6.10).

$$f^r = |\sigma^r - H^r \epsilon^{pl,r}| - f_y^r \leqslant 0 \tag{6.10}$$

With σ^r the axial strain in a reinforcement in the direction $(\overrightarrow{V_r})$, f_y^r the elastic limit for the reinforcements, and H^r the hardening modulus.

Reinforcement relaxation

According to [12],the reversible viscous strain can be modelled thanks to a Kelvin element:

$$\frac{\partial \epsilon^{r,k}}{\partial t} = \frac{1}{\tau^{r,k}} \left(\frac{\epsilon^e}{K} - \epsilon^{r,k} \right) \tag{6.11}$$

With K the rate of reversible viscous strain relatively to the elastic strain and $\tau^{r,k}$ the characteristic time for the reversible viscous strain which depend on the temperature:

$$\tau^{r,k} = \frac{\tau_{ref}^{r,k}}{k^{r,T}} \tag{6.12}$$

$$K = \frac{K_{ref}}{k^{r,T}} \tag{6.13}$$

With $\tau_{ref}^{r,k}$ the characteristic time fitted at reference temperature $T^{r,ref}$ and $k^{r,T}$ the thermal activation coefficient defined by equation (6.21). According to [12], the uni-axial permanent viscous strain $\epsilon^{r,m}$ derives from a non-linear Maxwell model analogue to the one used for the matrix [44]. The viscous strain is proportional to the current elastic strain, and inverse proportional to a consolidation coefficient Cc^r which affects the characteristic time τ^r if the viscous strain increases (6.14).

$$\frac{\partial \epsilon^{r,m}}{\partial t} = \frac{\epsilon^e}{\tau^r C c^r} \tag{6.14}$$

The consolidation coefficient depends on the current viscous strain as follows (6.15):

$$Cc^r = \frac{1}{k^r} \exp\left(\frac{1}{k^r}\frac{\epsilon^{r,m}}{\epsilon^e}\right) \tag{6.15}$$

In (6.15), k^r considers the coupling effects of temperature and mechanical non-linearities involved in the relaxation process.

$$k^r = k_{ref} k^{r,T} k^{r,m} \tag{6.16}$$

k_{ref} is a constant proportional to the delayed strain potential of material, it is a material constant fitted on experimental results. For instance, if a relaxation test is performed under a given stress level σ^{kr}, a delayed strain potential noted ϵ^{kr} can be obtained by curve fitting of the test result. The constant k_{ref} is linked to the previous parameters as follows:

$$k_{ref} = E\frac{\epsilon^{kr}}{\sigma^{kr}} \tag{6.17}$$

In (6.18) $k^{r,m}$ considers the non linear amplification of the relaxation rate with the loading level:

$$k^{r,m} = \frac{\mu^{cr}}{\mu^{cr} - \mu} \tag{6.18}$$

With μ the loading level defined as follows:

$$\mu = \frac{|\sigma^r|}{f_y^r} \tag{6.19}$$

In (6.18) μ^{cr} is a constant depending on the sensitivity of the reinforcement material to increase non-linearly its relaxation rate when the load increases; it is linked to a characteristic data χ^r called *relaxation non linearity factor*, defined such as the relaxation remains linear if $\chi^r = 1$ and becomes non-linear when $\chi^r > 1$:

$$\mu^{cr} = \frac{2}{3}\frac{\chi^r}{\chi^r - 1} \tag{6.20}$$

In (6.16), $k^{r,T}$ considers the effect of the temperature on the relaxation velocity. According to [46] the relaxation is accelerated by the temperature rising, and a coupling with the loading level exists since this amplification depends non-linearly of the applied stress. To consider this second coupling, the model [12] assumes the thermal activation multiplication of the delayed

strain potential ($k^{r,T}$) depends non linearly of the loading level through the thermal activation coefficient $A^{r,T}$:

$$k^{r,T} = \begin{cases} \exp\left(A^{r,T}\left(T - T^{r,ref}\right)^{n^r}\right) & \text{if } T > T^{r,ref} \\ \exp\left(-A^{r,T}\left(T^{r,ref} - T\right)^{n^r}\right) & \text{if } T \leqslant T^{r,ref} \end{cases} \tag{6.21}$$

T the absolute temperature, and $T^{r,ref}$ the reference temperature for which the relaxation characteristic time τ^r was fitted, $n^r \approx 1.216$ a fitted parameter.

$$A^{r,T} = A^{r,T}_{ref} \exp\left(\gamma^r \mu^{thm}\right) \tag{6.22}$$

In (6.22), $k^{TT}_{ref} \approx 1.5.10^{-4}$ (according to [12]) is a fitted constant to consider the effect of temperature on the relaxation rate , γ^r a material constant and μ^{thm} is a loading rate able to change the activation energy defined as follows:

$$\mu^{thm}\left(t + dt\right) = \max\left(\mu^{thm}(t), \mu(t + dt), \mu^{thr}\right) \tag{6.23}$$

$\mu^{thr} \approx 0.7$ is the minimal loading level able to change the activation energy. $\mu(t + dt)$ is given by (6.19).

6.3.2 Reinforcement-matrix bond

Perfect bond between matrix and reinforcements

Either a perfect bond or an imperfect bond can be considered between reinforcement and matrix. In case of perfect bond, the axial strain of the reinforcement is deduced from its approximated elongation:

$$\epsilon^r \approx \epsilon_r + \frac{1}{2}\gamma_r^2 \tag{6.24}$$

With ϵ_r the axial strain :

$$\epsilon_r = \overrightarrow{V^r}^t \bar{\bar{\epsilon}} \overrightarrow{V^r} \tag{6.25}$$

and γ_r the shear strain :

$$\gamma_r = ||\bar{\bar{\epsilon}}\overrightarrow{V^r} - \epsilon_r \overrightarrow{V^r}|| \tag{6.26}$$

Imperfect bond between matrix and reinforcements

If a sliding between the reinforcement and the matrix is possible, the reinforcement's strain cannot be directly deduced from the mechanical strain of the matrix. To assess the reinforcement strains the model uses a non local approximation of the reinforcement-matrix interaction. This approximation consists to consider that the total strain ϵ_r of each reinforcement can be assessed using a second gradient method (6.27). This implementation affects both the constitutive behaviour law and the finite element solver *(UNPAS.PROCEDUR in Castem software)*, since the reinforcement's total strains, (ϵ_r) is replaced in (6.9) by its non local associated variable $(\overline{\epsilon_r})$ deduced using (6.27).

$$\bar{\epsilon}_r - \frac{l^{cr}}{2}\frac{\partial^2 \bar{\epsilon}_r}{\partial x_r^2} = \epsilon_r \tag{6.27}$$

(6.27) is an Helmholtz equation for which the variational form has to be solved at each sub-step by the finite element solver. Concerning the variational form, if a thermal analogy is used to build the numerical model, it is necessary to consider an anisotropic equivalent conductivity for which a single non-null coefficient exits in the direction $\vec{V}^r$ (while the coefficients are null in the two orthogonal directions), and it is necessary to build as many Helmholtz formulations as there are reinforcement types. In (6.27) l_r^c is the characteristic length for the second gradient method applied to the reinforcements oriented in direction $\vec{V}^r$. This characteristic length depends on the shear bond behaviour law between reinforcement and matrix. It can be shown that if the bond behaviour is linear the characteristic length has the form:

$$l^{cr} = \sqrt{\frac{E^r D^r}{H^r}} \tag{6.28}$$

With E^r the stiffness of the reinforcement, D^r its equivalent diameter, and H^r the tangent stiffness of the bond defined as:

$$H^r = \frac{\partial \tau^{mr}}{\partial d^{mr}} \tag{6.29}$$

with τ^{mr} the shear stress supported by the bond and d^{mr} the sliding between the reinforcement and the matrix.

Note the Helmholtz formulation able to consider the matrix-reinforcement sliding is active only if the model is used in its non-local formulation. In this case the name of the internal variables $\bar{\epsilon}_r$ have to be specified by the user for each reinforcement for which the bond is considered non-perfect.

6.4 Cracks distribution along reinforcements

The minimal localized crack number n_i^c in the direction i of a finite element, depends on its dimension l_i in the direction $\overrightarrow{V_i}$. The minimal fracture energy released in this direction depends then directly on n_i^c as follows:

$$Gf_i = n_i^c Gf \tag{6.30}$$

For any other direction an interpolation of Gf is used:

$$Gf_{\overrightarrow{V}} = \overrightarrow{V}^T \mathbf{Gf} \overrightarrow{V} \tag{6.31}$$

With $\mathbf{Gf}$ a fracture energy tensor built as follows:

$$\mathbf{Gf} = \sum_{i=1}^{3} Gf_i \overrightarrow{V_i} \bigotimes \overrightarrow{V_i} \tag{6.32}$$

For an assumed stabilized crack process, the localized cracks number (6.35) depends on the maximal distance l_i^f (6.33) between two consecutive cracks. If a constant shear bond stress is assumed, it can be computed by (6.33) where D_i^{eq} the equivalent diameter of the reinforcements defined as the ratio of the cross section to the perimeter of the reinforcement.

$$l_i^f = 2\left(\frac{D_i^{eq}}{4}\right)\frac{R^t}{\tau^r}\left(\frac{1-\rho_i}{\rho_i}\right) \tag{6.33}$$

But when the reinforcement plastification occurs the crack formation is also limited by the straight anchorage length (6.34) of the reinforcements.

$$l_i^s = \frac{D_i^{eq}}{4}\frac{fy}{\tau^r} \tag{6.34}$$

With fy the reinforcement elastic limit.

$$n_i^c = \max\left(1, \frac{l_i}{l_i^f}, \frac{l_i}{2l_i^s}\right) \tag{6.35}$$

As, in a finite element, the fracture energy depends on the localized cracks number, the cracks opening computed by the model corresponds to a single of these possibly multiple cracks. The number of cracks in each main direction is also available in the internal variable list of the model.

Part III

Model using

Chapter 7

Model activation

The model can be used either in local formulation or in non-local formulation. The probabilistic scale effect (WL2 method) and the distributed reinforcements sliding in the matrix are available only in non-local formulation because they use the Helmholtz method implemented on purpose. So there are two ways to invoke the model in Castem:

- Local formulation without WL2, with reinfocement perfectly bond to the matrix
- Non Local formulation with WL2 and possibility to consider a sliding between ditributed reinforcements and matrix

7.1 Local formulation

The model is formulated to work in the context of 3 dimensions imposed strains: this formulation includes:

- 3 dimensions
- 2 dimensions with plain strain formulation
- 2 dimension with axi-symmetric formulation

For the two last modes, a parameter giving the out of plan dimension is needed, it is called:

- DIMZ in 2D plain strain
- DIMT in 2D axi-symmetry

If the mesh to be used is called vol1, the model activation is done as follows:

```
*model declaration from the mesh (vol1) for local formulation
mod1=MODELE vol1 MECANIQUE ELASTIQUE ISOTROPE
VISCOPLASTIQUE  FLUENDO3D;
*material declaration (see below)
*material declaration for damage and plasticity
mdam1=...
*material declaration for water effects
mwat1=...
...
*material declaration for reinforcement 1
mrenf1=...
*material chracteristics assemblage
mat1=matd1 ET mdam1 ET mwat1 ET mrag1 ET mdef1 ET mprob1 ET
marenf1 ;
```

7.2 Non Local formulation

The Helmholtz method has been implemented to consider non local formulation of WL2 and of the sliding reinforcements. As explained in chapter 5 and 6. The key word specifying the internal variables on which are applied the Helmholtz formulation are given in the model declaration, while the characteristic lengths corresponding to each of them are added in the material declaration. For WL2 the characteristic lenght is LCAR, for each reinforcement processed by the Helmholtz formulation theay are LCF1, LCF2...For instance the command lines below allow to apply the Helmholtz formulation for WL2 (variable XWL2) and for the first reinforcement (variable ENL1). Other reinfocement's variable are ENL2, ENL3...and can be added if needed.

```
*model declaration from the mesh (vol1) for non local formulation
mod1=MODELE vol1 MECANIQUE ELASTIQUE ISOTROPE
VISCOPLASTIQUE  FLUENDO3D 'NON_LOCAL' 'HELM'
'V_MOYENNE' ( 'MOTS' 'XWL2' 'ENL1') ;
*material declaration (see below)
*material declaration for damage and plasticity
mdam1=...
*material declaration for water effects
mwat1=...
*material declaration for CREEP
mcreep1=...
*material declaration for AAR
mrag1=...
*material declaration for DEF
mdef1=...
*material declaration for Weibull scale effect
mprob1=...LCAR 0.3;
*material declaration for reinforcement 1
mrenf1=...LCF1 0.1;
*material chracteristics assemblage
mat1=mdam1 ET mwat1 ET mcreep1 ET mrag1 ET mdef1 ET mprob1 ET
marenf1 ;
```

Note: if other internal variables have to be treated by the Helmholtz formulation the procedure 'PAS_HELM.PROCEDUR' of Cast3M has to be adapted. The treatment for LCAR et LCF1...are not the same. LCAR is based on a isotropic Helmholtz formulation while LCF1...use anisotropic ones, that is why the orientation vectors of reinforcements are needed in mrenf1.

Chapter 8

Data classified by physic phenomena ans associated command lines

8.1 Principle

In this chapter the material parameters are split in several sub-materials, all of them being associated to the model. Each sub-material corresponds to an aspect of the global behaviour law (damage, creep, reinforcement, scale effect, alkali reaction, delayed ettringite formation...), next all the sub-materials are assembled in a single material. This method allows to find more easily the parameters corresponding to each component of the behaviour law than if all the parameters were passed in a single instructions. More this method avoids to have too many command lines for the material definition.

8.2 Elasticity, strengths, plasticity and damage due to loading, link with hydration

8.2.1 Command lines

mdam1=MATE mod1 YOUN 30000. NU 0.2 RHO 2400. ALPH 1.0e-5 HYDR 0.8 HYDS 0.2 HREF 0.8 RT 3. EPT 1.1e-4 RC 40. EPC 2.0e-3 DELT 1. BETA 0.15 REF 4. EKDC 2.0e-3 GFT 1.0e-4 GFR 1.0e-4 DT80 0.15 TSTH 45. NREN 1.;
* In plain strain and axi-symmetric formulation the out of plane dimension must be added : DIMZ 0.1 or DIMT 0.1 (respectively) in the list above

8.2.2 Data list

Parameter	Symbol	Unit	Name	Value
Basic thermo-elasticity				
Young modulus	E	MPa	YOUN	30000.
Poisson ratio	ν	-	NU	0.2
Density	ρ	kg/m^3	RHO	2400.
Thermal dilation coefficient	α	-	ALPH	1.0e-5
Solidification				
Hydration advancement	ξ	-	HYDR	1.0
Solidification hydration threshold	$\xi^t h$	-	HYDS	0.2
Hydration reference for data	ξ^{ref}	-	HREF	0.8
Basic Plasticity				
Tensile strength	R_t	MPa	RT	3.
Strain at tension pick	ε_{Rt}^{pk}		EPT	1.0e-4
Uniaxial Compressive strength	R_c	MPa	RC	30.
Strain at uniaxial compression pick	ε_{Rc}^{pk}	-	EPC	2.0e-3
Drucker Prager confinement coefficient	δ	-	DELT	0.75
Dilatancy for non associated Drucker Prager plastic flow	β	-	BETA	0.15
Reclosure characteristic stress	$\tilde{\sigma}_{rcl}$	MPa	REF	4.
Damage associated to basic plasticity				
Characteristic plastic strain for Drucker Prager associated damage	$\varepsilon^{k,s}$ (3.22)	-	EKDC	1.0e-4
Fracture energy in tension	G_t^f	MJ/m^2	GFT	1.0e-4
Tensile crack reclosure energy	G_r^f	MJ/m^2	GFR	2.0e-4
Thermal Damage				
Thermal damage at 80 °C	D_{80}^T	-	DT80	0.15
Damage temperature threshold	θ_{thr}	°C	TSTH	45.
Reinforcement types number				
Number of types of reinforcements	N^r	-	NREN	$0 \rightarrow 5$

Table 8.1: Data for mechanical behaviour of the matrix

8.3 Effects of water: capillary effects, shrinkage and associated damage

8.3.1 Command lines

```
mwat1=MATE mod1 PORO 0.12 VW 0.12 BSHR 0.25 MSHR 40. TTRW
20. MVGN 0.5 CSHR 0. EKDW 1.0e-2 TTKW 40. HSHR 1.0e5 DCDW 0.0
KWRT 0.25 KWRC 0.10;
```

8.3.2 Data list

Parameter	Symbol	Unit	Name	Value
Capillary pressure effects				
Porosity	ϕ	m^3/m^3	PORO	0.12
Water content	ϕ^W	m^3/m^3	VW	0.12
Biot coefficient for shrinkage	b_{shr}	-	BSHR	0.25
Van Genuchten Modulus at reference temperature fir the capillary curve	M_{shr}^{ref}	MPa	MSHR	40.
Reference temperature for the capillary curve	$T^{w,ref}$	C	TTRW	20.
Van Genuchten exponent	m_{VG}	-	MVGN	0.5
Stress concentration factor for cracking criteria by capillary pressure	C^{shr}	-	CSHR	1.
Characteristic strain to link capillary induced strain and tensile damage	ϵ^{kdw}	-	EKDW	1.e-2
Characteristic temperature to consider effect of temperature on capillary pressure	T^{KW}	C	TTKW	40.
Hardening modulus for the evolution of local tensile strength to capillary pressure	H^w	MPa	HSHR	1.0e5
Exponent of $(1 - D^{tw})$ for coupling between damages due to capillary pressure and compression	α^W	-	DCDW	0.
Influence coefficient of capillary pressure on macroscopic tensile strength	$K^{W,Rt}$	-	KWRT	0.25
Influence coefficient of capillary pressure on macroscopic compressive strength	$K^{W,Rc}$	-	KWRC	0.10

Table 8.2: Data for mechanical effects of capillary water

8.4 Creep

8.4.1 Command lines

```
mcreep1=MATE mod1 TTRF 20. TAUK 0.7 YKSY 3.75 TAUM 14. EKFL
0.9e-4 XFLU 2. NRJM 20000. DFMX 0.10 KDTT 0.0 ;
```

8.4.2 Data list

Parameter	Symbol	Unit	Name	Value
Creep				
Reference temperature for creep model parameters	θ_{ref}	°C	TTRF	20.
Characteristic time for Kelvin module	τ^K_{ref}	Day	TAUK	0.7
Kelvin stiffness / Young module Ratio	ψ^K		YKSY	3.75
Characteristic time for Maxwell Module	τ^M_{ref}	Day	TAUM	14.
Creep potential characteristic strain	ε^M_{ref}	-	EKFL	0.9e-4
Non linear creep potential multiplicator at $66\%R_C, (\geqslant 1)$	χ^M	-	XFLU	2.
Activation energy for creep potential amplification in temperature	E^M_A	$J/mol.K$	NRJM	20000.
Maximal creep damage	D^C_{max}	-	DFMX	0.10
Transient Thermal creep constant	k^{dtt}	-	KDTT	0.

Table 8.3: Data for creep of the matrix

8.5 Alkali aggregate reaction

8.5.1 Command lines

```
mrag1=MATE mod1 VRAG 0. TRAG 120. SRSR 0.5 NRJR 40000. HRAG
1500. KRAG 2000. EKDG 3.0e-3 VVRG 0. CRAG 0.5 TTRG 38. DCDG
0.15;
```

8.5.2 Data list

Parameter	Symbol	Unit	Name	Value
Alkali aggregate reaction AAR				
Maximal AAR product volume ratio	ϕ_{aar}^{∞}	m^3/m^3	VRAG	0.
Characteristic time for AAR reaction	τ_{ref}^{aar}	$days$	TRAG	120.0
Water saturation threshold to activate AAR	$S_r^{th,aar}$	-	SRSR	0.5
Activation energy for AAR kinetic	E^{aar}	J/Mol	NRJR	40000.0
Hardening modulus of the tensile strength used in the AAR cracking criteria	H^{AAR}	MPa	HRAG	1500.
Compressibility modulus for AAR	K^{AAR}	MPa	KRAG	2000.
Characteristic strain to link AAR strain and AAR damage in tension	ϵ^{kdg}	-	EKDG	3.0e-3
Void filled by tge AAR gel at free cracking	$\phi^{V,AAR}$	-	VVRG	0.
Stress concentration factor for AAR	k^{AAR}	-	CRAG	0.5
Reference temperature of AAR kinetic paramter	$T^{ref,AAR}$	C	TTRG	38.
Exponent of $(1 - D^{gw})$ for coupling between damages due to AAR pressure and compression	$\alpha^A AR$	-	DCDG	0.15

Table 8.4: Data for AAR

8.6 Delayed Ettringite Formation (DEF)

8.6.1 Command lines

```
mdef1=MATE mod1 VDEF 5.0e-2 SSAD 0.7 TTKD 80. TTKF 70. TTRP
20. TDID 3. TFID 1.5 TPRD 30. NRJD 70000. NRJF 180000. NRJP
40000. NALD 0.3 NAKD 0.28 NABD 0.92 SRSD 0.95 EXND 0.18 EXMD 3.
EKDS 3.0e-3 HDEF 1500. KDEF 33000. VVDF 0.1 CDEF 0.5 DCDS 0.15;
```

8.6.2 Data list

Parameter	Symbol	Unit	Name	Value
Delayed Ettringite Formation				
Maximal amount of DEF	ϕ_{def}^{∞}	m^3/m^3	VDEF	0.05
Sulphate/Aluminates moles number ratio	ρ	–	SSAD	0.7
Mole number of sulphates per unit volume	S_{imp}^{c}	Mol/m^3	NSUL[1]	170.
Characteristic temperature for sulphoaluminate dissolution	$T^{Diss,ref}$	°C	TTKD	80.
Minimal temperature to start aluminates fixation	$T^{th,Fix}$	°C	TTKF	70.
Reference temperature for the characteristic time of DEF precipitation	$T^{ref,Prec}$	°C	TTRP	20.
Characteristic time for the dissolution of sulphoaluminates	$\tau^{Diss,ref}$	$days$	TDID	3.
Characteristic time for the fixation of aluminates in hydro-garnets	$\tau^{Fix,ref}$	$days$	TFID	1.5
Characteristic time of precipitation	τ^{Prec}	$days$	TPRD	120.
Activation energy for the dissolution of sulfoaluminates	$E^{a,Diss}$	J/mol	NRJD	70000.
Activation energy for the fixation of aluminates	$E^{a,Fix}$	J/mol	NRJF	180000.
Activation energy for the precipitation	$E^{a,Prec}$	J/mol	NRJP	40000.
Free alkali concentration in pore solution	Na	mol/l	NALD	0.3
Reference Alkali concentration for laws depending on free alkali concentration	Na^{k}	mol/l	NAKD	0.28
Alkali concentration blocking the DEF precipitation	$Na^{th,def}$	mol/l	NABD	0.92
Characteristic water saturation rate for the kinetic term of DEF precipitation	$S_r^{th,def}$	–	SRSD	0.95
Exponent of coupling law for DEF dissolution temperature	n	–	EXND	0.18
Exponent of coupling law for DEF precipitation and aluminate fixation	m	–	EXMD	3

[1]Give either VDEF or NSUL, if the two variables are imposed the VDEF is used to compute the molar volume of DEF else the real volume is used and the moles number computed according to NSUL and SSAD

Parameter	Symbol	Unit	Name	Value
Chracterirstic strain to link DEF strain and induced damage	ϵ^{kd}	-	EKDS	3.0e-3
Hardening module for the tensile strength evolution in DEF criterion	H^{DEF}	MPa	HDEF	5000.
Compressibility of ettringite	K^{DEF}	MPa	KDEF	33000.
Void filled by ettringite at free cracking	b^{DEF}	-	VVDF	0.
Stress concentration factor for the DEF	k^{DEF}	-	CDEF	0.5
Exponent of $(1 - D^{tDEF})$ for coupling between damages due to capillary pressure and compression	$\alpha^{D}EF$	-	DCDS	0.15

Table 8.5: Data for DEF

8.7 Probabilistic scale effect (WL2 method)

8.7.1 Command lines

Before building the material list, it is necessary to compute the VMAX variable which is a non local field (vmax1 in the following example). This field uses the non local characteristic lenght lc1, which must be the same than in the material:

```
* characteristic lenght for WL2 method
lc1=0.50;
*connectivity for NLOC operator used to assess VMAX
conn1 = 'CONN' mod1 (lc4*(2.*(2.**0.5)))'NORMAL' 'INTERIEUR';
*other possible symetries: 'DROITE' p1 p2 or 'AXE VERTICAL'...;
chp1=manu chpo vol1 'SCAL' (1.);
un1=chan 'CHAM' chp1 mod1 'STRESSES' 'CARACTERISTIQUES';
un2=exco 'SCAL' un1 'VMAX';
lism1=mots 'VMAX';
*option NODI to avoid division in NLOC operator
vmax1=NLOC un2 conn1 lism1 'NODI';
```

Then, the material can be defined as follows:

```
mprob1=MATE mod1 VREF 2.e-4 CVRT 0.15 VMAX vmax1 LCAR lc1;
```

8.7.2 Data list

Parameter	Symbol	Unit	Name	Value
Weibull scale effect with WL2 method				
Reference volume for the tensile strength	V^{eq}	m^3	VREF	2.e-4
Coefficient of variation of the tensile strength	C^v	-	CVRT	0.15
Maximal equivalent volume field	V^{max}	m^3	VMAX	-[2]
Characteristic length for the Wl2 method	l^c_{WL2}	m	LCAR[3]	0.5

Table 8.6: Data for Weibull scale effect

[2]Scalar field to built before the material delaration with the NLOC command
[3]Available only if the model is non local with the Helmholtz formulation activate see 7.2

8.8 Reinforcements

Note, the number of reinforcements NREN can be given anywhere, but as when NREN=0 (none reinforcements) the information is given in the material for the matrix, it can be kept there, so it is recall in the table below but given in the first material (see 8.2.1).

8.8.1 Command lines

```
matren1=MATE mod1 ROA1 0.01 DEQ1 0.01 YOR1 2.0e5 SYR1 1800.
TYR1 6. VR11 0. VR12 0. VR13 1. HPL1 5.0e3 TMR1 0.1 TKR1 0.1 YKY1
100. EKR1 1.0e-4 SKR1 1260. ATR1 1.5e-4 CTM1 4.8 XNR1 1.216 XFL1
2.55 MUS1 0.7 PRE1 800. TTR1 20. LCF1 0.15 ;
```

These command lines can be copied as often as needed to specify data for the possible other reinforcements. In this case the suffix "1" of each data is replaced by the numerous of the reinfocement (until 5 maximum).

8.8.2 Data list

Parameter	Symbol	Unit	Name	Value
Distributed reinforcements behaviour laws				
If more than one reinforcement, duplicate the data list bellow replacing 1 by $I = 1..NREN$				
Reinforcement's number	N^r	–	NREN	$\in [0..5]$[4][5]
Reinforcement density direction 1	ρ^{r1}	–	ROA1	0.01
Equivalent diameter direction 1	Deq^{r1}	m	DEQ1	0.01
Reinforcement Young modulus	E^{r1}	MPa	YOR1	2.e5
Reinforcement elastic limit	fy^{r1}	MPa	SYR1	1800.
Bond stress interface reinforcement matrix	τ^{r_1}	MPa	TYR1	6.0
Projection of the normalized direction of Reinforcement on the first fix axe	e_1^{r1}	–	VR11	1.0
Projection of the normalized direction of Reinforcement on the second fix axe	e_2^{r1}	–	VR12	0.0
Projection of the normalized direction of Reinforcement on the thirst fix axe	e_3^{r1}	–	VR13	0.0
Reinforcement Hardening modulus	H_1^r	MPa	HPL1	5000
Reinforcement Irreversible Relaxation characteristic time	τ^r	Day	TMR1	0.1
Reinforcement Rreversible Relaxation characteristic time	τ^r	Day	TKR1	0.1
Reinforcement Reversible Relaxation Reduction coefficient at T_{ref}	K_{ref}	–	YKY1	100.

[4]Possibility to add more then 5 reinforcement's types recompiling IDVISC, CFLUENDO3d with $NBRENF3D \neq 5$,and add corresponding internal variables in IDVAR4

[5]NREN already given in material definition for the matrix, do not repeat this date which is single for the model

Parameter	Symbol	Unit	Name	Value
Characteristic strain for reinforcement relaxation	ϵ^{kr}	–	EKR1	1.e-4
Characteristic stress for the fitting of ϵ^{kr}	σ^{kr}	MPa	SKR1	1260.
Reference value of the thermal activation coefficient (6.22)	$A^{r,T}_{ref}$	–	ATR1	1.5e-4
Coupling coefficient for effect of stress on activation energy	γ^r	–	CTM1	4.8
Non linear relaxation coefficient	χ^r	–	XFL1	2.55
Exponent of temperature in thermal activation of relaxation (6.21)	n^r	–	XNR1	1.216
Loading level threshold above which the thermal activation depends on loading (6.22)	μ^{th}	–	MUS1	0.7
Initial pre-tress (imposed as initial stress at first step)	σ^r_0	MPa	PRE1	800.
Reference temperature for the dtermination of τ^r	$T^{r,ref}$	°C	TTR1	20.
Characteristic length for the non local formulation of sliding interfaces (reinforcement type number 1)	$l^c_{r,1}$	m	LCF1[6]	0.15

Table 8.7: Data for the reinforcements definition

[6]Used only if non local Helmholtz formulation activate for the variable ENL1, see 7.2

Chapter 9

Results

9.1 Internal variables management

9.1.1 Limitation of computer's memory used

As each material embedded in the model has between ten and twenty internal variables, and as each variable is stored in the memory of the computer at each Gauss point of each element and each time step, the size of the memory occupied by the internal variables of the model can be significant for meshes with a great number of elements and great number of time steps. So it is advisable to save only the internal variables at important time steps using the options TAB.TEMPS_CALCULES for the list of computed time step, TAB.TEMPS_SAUVES for the list of time steps to save, and TAB.TEMPS_SAUVEGARDES for the sub list of time steps to store in a file in order to recover them later, either to continu the calculus, or to access them to exploit results.

9.1.2 Access to an internal variable at a given time

Once the calculus achieved, users can recover any internal variables of the model at any stored time step. To obtain an internal variable, for instance the maximal crack opening stored in the internal variable WL0 at a given time *temps1* corresponding to iteration i1, it is convenient to process as follows:

```
*print the list of time stored by PASAPAS in tab1 to identify the time step
number i1, then affect i1
LIST tab1.TEMPS ;
*choice of time step number i1 and plot of internal variable chosen at this
time step number
i1=...;
TRAC ( EXCO WL1 tab1.variables_internes.i1) mod1 ;
```

9.2 Total Stresses and stresses by phases

In the case the reinforcement are used (NREN>0), it is important to note that TAB1.CONTRAINTES provided by CASTEM supplies the total stresses (matrix plus reinfocements); the stresses in

the matrix alone or in the reinforcements alone are stored in the internal variables listed below. Specifically the stresses in the matrix are call SIM1..6 (see 9.1) and in reinfocement SRF1..5 (see 9.11).

9.3 Internal variables for mechanical state in the matrix

9.3.1 Strains

The generic numerotation used to store the strains and the stresses are such that the corresponding tensor in the global base of the mesh. For instance the elastic strains stored in the pseudo vector $EPE1 \rightarrow 6$ corresponds to the following matrixs:

- If the problem is three-dimensional or in plain strain(global base (xyz)):

$$\begin{bmatrix} EPE1 & EPE4/2 & EPE5/2 \\ EPE4/2 & EPE3 & EPE6/2 \\ EPE5/2 & EPE6/2 & EPE3 \end{bmatrix} = \begin{bmatrix} \epsilon^e_{xx} & \gamma^e_{xy}/2 & \gamma^e_{xz}/2 \\ \gamma^e_{xy}/2 & \epsilon^e_{yy} & \gamma^e_{yz}/2 \\ \gamma^e_{xz}/2 & \gamma^e_{yz}/2 & \epsilon^e_{zz} \end{bmatrix} \tag{9.1}$$

- If the problem is axi-symmetric (global base rzθ):

$$\begin{bmatrix} EPE1 & EPE4/2 & EPE5/2 \\ EPE4/2 & EPE3 & EPE6/2 \\ EPE5/2 & EPE6/2 & EPE3 \end{bmatrix} = \begin{bmatrix} \epsilon^e_{rr} & \gamma^e_{rz}/2 & \gamma^e_{r\theta}/2 \\ \gamma^e_{rz}/2 & \epsilon^e_{zz} & \gamma^e_{z\theta}/2 \\ \gamma^e_{r\theta}/2 & \gamma^e_{z\theta}/2 & \epsilon^e_{\theta\theta} \end{bmatrix} \tag{9.2}$$

Number	Name
Elastic strains	
2	EPE1
3	EPE2
4	EPE3
5	EPE4
6	EPE5
7	EPE6
Drucker Prager plastic strains	
20	EPC1
21	EPC2
22	EPC3
23	EPC4
24	EPC5
25	EPC6
Tension plastic strains	
26	EPT1
27	EPT2
28	EPT3
29	EPT4
30	EPT5
31	EPT6

Table 9.1: Internal variables for strains in the matrix

9.3.2 Stresses

The numeration is analogous to the strains one.

Number	Name
Effective stresses in the solid part of the matrix	
50	SIG1
51	SIG2
52	SIG3
53	SIG4
54	SIG5
55	SIG6
Total Stresses in the matrix	
62	SIM1
63	SIM2
64	SIM3
65	SIM4
66	SIM5
67	SIM6

Table 9.2: Internal variables for Stresses in the matrix

9.3.3 Damages

Only the mechanical and global damage are given here. Other damages due to water, AAR or DEF are given in the corresponding section of this chapter. The suffix 0 means that this is the first main value of a second order tensor.

Number	Name
Thermal damage	
77	DTHE
Pre peak damage	
79	DTPP
Equivalent plastic strain (Drucker Prager)	
94	EPLC
Tensile damage (global)	
95	DTRA
Compressive damage (global)	
96	DCOM
Error on fracture energy to avoid snap back	
110	ERGF
Current principal Eigenvalues of tensile damages	
111	DTM0
Compressive and Shear Damage Drucker Prager	
115	DCM0
Localized tensile damage	
119	DTL0

Table 9.3: Internal variables for mechanical damage

9.3.4 Cracking

The numeration is the same than for strains. The suffix 0 means this the maximal eigenvalue of a tensor.

Number	Name
Crack opening (from plastic strains)	
97	WPL1
98	WPL2
99	WPL3
100	WPL4
101	WPL5
102	WPL6
Maximal cracks opening (versus time)	
103	WPX1
104	WPX2
105	WPX3
106	WPX4
107	WPX5
108	WPX6
Crack opening (Current principal crack opening)	
109	WPL0

Table 9.4: Internal variables for localized cracking

9.3.5 Others variables

Number	Name
Hydration used	
68	HYDF
Indicator first step passed	
1	PPAS

9.4 Internal variables for creep

Number	Name
Kelvin strains	
8	EPK1
9	EPK2
10	EPK3
11	EPK4
12	EPK5
13	EPK6
Maxwell strains	
14	EPM1
15	EPM2
16	EPM3
17	EPM4
18	EPM5
19	EPM6
Creep damage	
78	DFLU
Kelvin effective stresses	
56	SKE1
57	SKE2
58	SKE3
59	SKE4
60	SKE5
61	SKE6

Table 9.6: Internal variables for CREEP

9.5 Internal variables for the capillary effect of liquid water

Number	Name
Capillary pressure plastic strains	
32	EPW1
33	EPW2
34	EPW3
35	EPW4
36	EPW5
37	EPW6
Liquid water volume used	
69	VWAT
Porosity used	
70	VPOR
Biot coefficient used for liquid water	
80	BWAT
Water pressure	
81	PWAT
Capillary tensile damage	
112	DTW0
Capillary Compressive damage	
116	DCW0

Table 9.7: Internal variables for capillary effects

9.6 Internal variables for AAR

Number	Name
AAR plastic strains	
38	EPG1
39	EPG2
40	EPG3
41	EPG4
42	EPG5
43	EPG6
Biot coefficient used for AAR	
82	BGEL
AAR pressure	
83	PGEL
AAR advancement	
86	AGEL
AAR tensile damage	
113	DTG0
Compressive due to AAR	
117	DCG0

Table 9.8: Internal variables for AAR

9.7 Internal variables for DEF

Number	Name
DEF plastic strains	
44	EPS1
45	EPS2
46	EPS3
47	EPS4
48	EPS5
49	EPS6
Biot coefficient used for DEF	
84	BAFT
DEF pressure	
85	PAFT
Chemical species involved in DEF	
87	AFT1
88	AFM1
89	ATIL
90	STIL
91	AFT2
DEF advancement and volume	
92	ADEF
93	VAFT
DEF tensile damage	
114	DTS0
Compressive due to DEF	
118	DCS0

Table 9.9: Internal variables for DEF

9.8 Internal variables for Weibull scale effect

Number	Name
Non local variable for Weibull (WL2) method	
71	XWL2
Loading rate used for Weibull method	
72	TWL2
Mawimum of XWL2	
73	MXWL
Maximal loading rate used for Weibull method	
74	MTWL
Maximal Localized damage in tension	
75	DTMX
Scale effect coefficient computed by Weibull method	
76	CWRT

Table 9.10: Internal variables for Weibull scale effect

9.9 Internal variables for the reinforcements

The list below is given for reinforcement number 1. To access to another reinforcement replace 1 by its number.

Number	Name
Axial strain in reinforcement 1	
120	ERT1
Variable used for non local strain in reinforcement	
121	ENL1
Plastic strain in reinforcement	
122	ERP1
Axial stress in reinforcement	
123	SNR1
Maxwell strain in reinforcement	
124	ERM1
Maximal Loading rate in reinforcement	
125	MUR1
Kelvin strain in reinforcements	
126	ERK1

Table 9.11: Internal variables for the reinforcements

This table is repeated 4 times replacing "1" by the reinforcement number, adding 7 internal variables for each one. Consequently, the total number of internal variables for all the materials embedded in the model is $126 + 4 \times 7 = 154$. Each one is stored in a field at each time step to save.

Part IV

References

Bibliography

[1] Mahamad Al Shamaa. *Etude du risque de développement d'une réaction sulfatique interne et de ses conséquences dans les bétons de structure des ouvrages nucléaires.* PhD thesis, 2012.

[2] Mohamad Al Shamaa, Stéphane Lavaud, Loic Divet, Georges Nahas, and Jean Michel Torrenti. Coupling between mechanical and transfer properties and expansion due to DEF in a concrete of a nuclear power plant. *Nuclear Engineering and Design*, 266:70–77, 2014.

[3] V. Baroghel-Bouny, M. Mainguy, T. Lassabatere, and O. Coussy. Characterization and identification of equilibrium and transfer moisture properties for ordinary and high-performance cementitious materials. *Cement and Concrete Research*, 29(8):1225–1238, aug 1999.

[4] ZP Bazant, Gianluca Cusatis, and Luigi Cedolin. Temperature effect on concrete creep modeled by microprestress-solidification theory. *Journal of engineering mechanics*, (June):691–699, 2004.

[5] X. Brunetaud, R. Linder, L. Divet, D. Duragrin, and D. Damidot. Effect of curing conditions and concrete mix design on the expansion generated by delayed ettringite formation. *Materials and Structures*, 40(6):567–578, aug 2006.

[6] Raphaël Bucher, Alain Sellier, Jérôme Verdier, and Thierry Vidal. Effet de la microfissuration de séchage sur les propriétés mécaniques et de transfert des matériaux cimentaires. Technical report, LMDC Internal Report, Toulouse, 2016.

[7] Laurie Buffo-Lacarriere and Alain Sellier. Chemo-mechanical modelling requirements for the assessment of concrete structure service life. *Journal of Engineering Mechanics (ASCE)*, 37(9):625–633, 2011.

[8] H. Cagnon, T. Vidal, A. Sellier, X. Bourbon, and G. Camps. Drying creep in cyclic humidity conditions. *Cement and Concrete Research*, 76:91–97, oct 2015.

[9] Bruno Capra and Alain Sellier. Orthotropic modelling of alkali-aggregate reaction in concrete structures : numerical simulations. *Mechanics of Materials*, 6(December), 2002.

[10] Ignacio Carol and ZP Bazant. Damage and plasticity in microplane theory. *International Journal of Solids and Structures*, 34(29):3807–3835, oct 1997.

[11] Ponleu Chhun. *Modélisation du comportement thermo- hydro -chemo- mécanique de s enceinte s de confinement nucléaire en béton armé -précontraint.* PhD thesis, Université de Toulouse, INSA, UPS, 2017.

[12] Ponleu Chhun, Alain Sellier, Laurie Lacarriere, Sylvain Chataigner, and Laurent Gaillet. Incremental modeling of relaxation of prestressing wires under variable loading and temperature. *Construction and Building Materials*, 163:337–342, feb 2018.

[13] O Coussy. *Poromechanics*. Wiley, 2004.

[14] René De Borst and Jerzy Pamin. Gradient plasticity in numerical simulation of concrete cracking. *European Journal of Mechanics - A/Solids*, 15(2):295–320, 1996.

[15] G. De Schutter and L. Taerwe. Towards a more fundamental non-linear basic creep model for early age concrete. *Magazine of Concrete Research*, 49(180):195–200, sep 1997.

[16] Belay Zeleke Dilnesa, Barbara Lothenbach, Guillaume Renaudin, Adrian Wichser, and Dmitrii Kulik. Synthesis and characterization of hydrogarnet Ca 3 (AlxFe1-x)2(SiO4)y(OH)4(3-y). *submited to ccr*, 2014.

[17] D. C. Drucker and W. Prager. Soil mechanics and plastic analysis for limit design. *Quarterly of Applied Mathematics*, 10(2):157–165, 1952.

[18] K. S. Gopalakrishnan, Adam M. Neville, and Amin Ghali. Creep Poisson's Ratio of Concrete Under Multiaxial Compression. *ACI Journal proceedings*, 66(12):1008–1019, 1969.

[19] A Hillerborg, M Modeer, and PE Peterssonn. Analysis of crack formation and crack growth in concrete by means of fracture mechanics and finite elements. *Cement and Concrete Research*, 6:773–782, 1976.

[20] AD Jefferson. Craft–a plastic-damage-contact model for concrete. I. Model theory and thermodynamic considerations. *International Journal of Solids and Structures*, 40(22):5973–5999, nov 2003.

[21] L Kachanov. *Introduction tp continuum damage mechanic*. Martinus Nijhoff Publishers, P.O Box 163. 300 AD Dordrecht, The Netherlands, 1986.

[22] Badreddine Kchakech. *Etude de l ' influence de l ' échauffement subi par un béton sur le risque d ' expansions associées à la Réaction Sulfatique Interne*. PhD thesis, Paris Est, 2015.

[23] Christian LaBorderie, Claire Lawrence, and Abdellah Menou. Approche mésoscopique du comportement du béton. *European Journal of Environmental and Civil Engineering*, pages 1–16, 2007.

[24] Wahid Ladaoui. *Etude expérimentale du comportement Thermo-HydroMécanique à long terme des BHP destinés aux ouvrages de stockage des déchets radioactifs*. PhD thesis, Université de Toulouse, 2010.

[25] Wahid Ladaoui, Thierry Vidal, Alain Sellier, and Xavier Bourbon. Analysis of interactions between damage and basic creep of HPC and HPFRC heated between 20 and 80 ÂřC. *Materials and Structures*, 46:13–23, jul 2013.

[26] J Lemaitre and JL Chaboche. *Mécanique des matériaux solides*. Dunod, Paris, 1985.

[27] J Lemaitre and JL Chaboche. *Mécanique des matériaux solides*. Dunod, 1985.

[28] J Mazars. A description of micro- and macroscale damage of concrete structures,. *Engineering fracture mechanics*, 25(5-6):729–737, 1986.

[29] Pierre Morenon, Stéphane Multon, Alain Sellier, Etienne Grimal, François Hamon, and Eric Bourdarot. Impact of stresses and restraints on ASR expansion. *Construction and Building Materials*, 140:58–74, 2017.

[30] Michael Ortiz. A constitutive therory for the inelastic behvior of concrete. *Mechanics of Materials*, 4:67–93, 1985.

[31] Gilles Pijaudier-Cabot and ZP Bazant. Nonlocal damage theory. *Journal of Engineering Mechanics*, 113:1512–1533, 1987.

[32] Z. Pijaudier-Cabot, G., Bazant. Nonlocal damage theory. *Journal of Engineering Mechanics*, 113:1512–1533, 1987.

[33] S. Poyet, A. Sellier, B. Capra, G. Thèvenin-Foray, J.M. Torrenti, H. Tournier-Cognon, and E. Bourdarot. Influence of water on alkali-silica reaction: Experimental study and numerical simulations. *Journal of materials in civil engineering*, 18(July/August):588, 2006.

[34] Harifidy Ranaivomanana. *Transferts dans les milieux poreux réactifs non saturés : application à la cicatrisation de fissure dans les matériaux cimentaires par carbonatation*. PhD thesis, Université de Toulouse, 2010.

[35] Marie Salgues, Alain Sellier, Stéphane Multon, Eric Bourdarot, and Etienne Grimal. DEF modelling based on thermodynamic equilibria and ionic transfers for structural analysis. *European Journal of Environmental and Civil Engineering*, pages 1–26, 2014.

[36] A. Sellier, G. Casaux-Ginestet, L. Buffo-Lacarrière, and X. Bourbon. Orthotropic Damage Coupled with Localised Crack Reclosure Processing. Part I: Constitutive Laws. *Engineering Fracture Mechanics*, 97l(January):148–167, oct 2013.

[37] A. Sellier, G. Casaux-Ginestet, L. Buffo-Lacarrière, and X. Bourbon. Orthotropic Damage Coupled with Localized Crack Reclosure Processing. Part II: Applications. *Engineering Fracture Mechanics*, 97(January):168–185, oct 2013.

[38] Alain Sellier. Modélisation probabiliste pour un chargement THM, Prise en compte des effets d'échelle aléatoires induits par le retrait différentiel pâte granulat. Groupe de Travail 4 du Projet de recherche ANRT Mefisto. Technical report, Université de Toulouse - INSA/UPS/LMDC, Toulouse, 2012.

[39] Alain Sellier and Laurie Buffo-Lacarrière. Vers une modélisation simple et unifiée du fluage propre, du retrait et du fluage en dessiccation du béton. *European Journal of Environmental ...*, 13(10):1161–1182, 2009.

[40] Alain Sellier, Laurie Buffo-Lacarrière, Stéphane Multon, Thierry Vidal, and Xavier Bourbon. Nonlinear basic creep and drying creep modelling. In Rossi & Tailhan, editor, *SSCS conference*, Aix en Provence, 2012.

[41] Alain Sellier and Bruno Capra. Modélisation physico-chimique de la réaction alcali-granulat: apport au calcul des structures dégradées. *Revue Française de Génie Civil*, 1(3):445–481, jan 1997.

[42] Alain Sellier and Alain Millard. Weakest link and localisation WL 2 : a method to conciliate probabilistic and energetic scale effects in numerical models. *European Journal of Environmental and Civil Engineering*, 18(10):1177–1191, apr 2014.

[43] Alain Sellier and Stéphane Multon. Modélisation simplifiée de la réaction sulfatique interne, Rapport interne LMDC /2016-2. Technical report, LMDC/INSA/UPS, Toulouse, 2016.

[44] Alain Sellier, Stéphane Multon, Laurie Buffo-lacarrière, Thierry Vidal, Xavier Bourbon, and Guillaume Camps. Concrete creep modelling for structural applications : non-linearity , multi-axiality , hydration , temperature and drying effects. *Cement and Concrete Research*, 79:301–315, 2016.

[45] Thomas Stablon, Alain Sellier, Nathalie Domede, Bernard Plu, and Luc Dieleman. Influence of building process on stiffness: numerical analysis of a masonry vault including mortar joint shrinkage and crack re-closure effect. *Materials and Structures*, nov 2011.

[46] Wiem Toumi Ajimi, Sylvain Chataigner, Yannick Falaise, and Laurent Gaillet. Experimental investigations on the influence of temperature on the behavior of steel reinforcement (strands and rebars). In International Conférence on Concrete in Severe Conditions, editor, *CONSEC 2016*, page 8, 2016.